CAPITAL UNIVERSITY OF SCIENCE AND TECHNOLOGY,
ISLAMABAD

Numerical simulation of mixed convective flow in an inclined channel with cavity with Cu-water nanofluid in porous medium

by

Ayesha Farooq

A thesis submitted in partial fulfillment for the
degree of Master of Philosophy

in the
Faculty of Computing
Department of Mathematics

March 2017

Numerical simulation of mixed convective flow in an inclined channel with cavity with Cu-water nanofluid in porous medium

by
Ayesha Farooq
MMT151006

Dr. Shafqat Hussain
(Thesis supervisor)

Dr. Muhammad Sagheer
(Internal Examiner)

Dr.

(External Examiner)

Dr. Muhammad Sagheer

(Head of Department, Mathematics)

Dr. Muhammad Abdul Qadir
(Dean, Faculty of Computing)

DEPARTMENT OF MATHEMATICS
CAPITAL UNIVERSITY OF SCIENCE AND TECHNOLOGY,
ISLAMABAD
March 2017

Certificate of Approval

This is certify that **Ayesha Farooq**, Reg. NO. MMT151006 has incorporated all suggestion, clarification and explanation by the thesis supervisor Dr. Shafqat Hussain as well as external evaluator and internal examiner at capital university of science and technology islamabad. The research work titled her Thesis is: **Numerical simulation of mixed convective flow in an inclined channel with cavity with Cu-water nanofluid in porous medium.**

Forwarded for necessary action

Dr. Shafqat Hussain

(Thesis supervisor)

Declaration of Authorship

I,"Ayesha Farooq", declare that this thesis titled, 'Numerical simulation of mixed convective flow in an inclined channel with cavity with Cu-water nanofluid in porous medium' and the work presented in it are my own. I confirm that:

- This work was done wholly or mainly while in candidature for a research degree at this University.
- Where any part of this thesis has previously been submitted for a degree or any other qualification at this University or any other institution, this has been clearly stated.
- Where I have consulted the published work of others, this is always clearly attributed.
- Where I have quoted from the work of others, the source is always given. With the exception of such quotations, this thesis is entirely my own work.
- I have acknowledged all main sources of help.
- Where the thesis is based on work done by myself jointly with others, I have made clear exactly what was done by others and what I have contributed myself.

Ayesha Farooq
MMT151006

Signed: _____

Date: _____

"God used the beautiful mathematics in creating the world"

Paul Dirac

CAPITAL UNIVERSITY OF SCIENCE AND TECHNOLOGY, ISLAMABAD

Abstract

Faculty of Computing
Department of Mathematics

Master of Philosophy
by
Ayesha Farooq

A numerical study has been carried out in the analysis of two dimensional, incompressible and steady mixed convective flow in an inclined channel with cavity. Cavity is filled with Cu-water nanofluid saturated with porous medium using the Brinkman Darcy Model. The temperature at the left wall of the cavity is considered as T_H and inlet temperature of the channel is T_C while rest of walls are at adiabatic. The governing equations are discretized in space using finite element pair $Q_2/{P_1}^{disc}$ which let to third and second order accuracy in the L_2-norm for velocity/temperature and pressure, respectively. The discretized system of non-linear equations are treated by Picard method and the linear subproblems are solved by means of Gaussian elimination method. The effects of physical parameters in specific ranges such as Richardson number (0.01 - 10), Darcy number (10^{-4} - 10^{-1}), inclination angle (0^o - 270^o) and solid volume fraction (0 - 0.06) on the flow are presented. The obtained results are shown by isotherms and streamlines. Moreover, graphical results are illustrated to observe the intensity of ϕ by ranging the inclination angle from (0^o - 360^o). It is observed that increment of average Nusselt number depends on the variation of Darcy number and Grashof number.

Acknowledgements

All of the appreciations are for ALLAH who is most ever lasting and the sustainer of this universe. Everything belong to him whatever in the heavens and whatever on the earth. Countless respect and endurance for Prophet Muhammad (Peace be upon him), the fortune of knowledge, who took the humanity out of ignorance and shows the rights path.

I would first like to thank my supervisor **Dr. Shafqat Hussain**, Associate Professor, Capital University of Science and Technology, Islamabad who suggested the problem. The doors towards supervisor were always open whenever I ran into a trouble spot or had a question about my research or writing. He consistently allowed this paper to be my own work, but steered me in the right the direction whenever he thought I needed it. I deem it as my privilege to work under his able guidance. Also special thanks to my teacher **Dr. M. Sagheer**, Associate Professor, Capital University of science and Technology and to **Dr. Rashid Ali**, Assistant Professor, Capital University of science and Technology, Isb.

I would also like to thank the experts who were involved in the validation survey for this research, **Mr. Khalid Mehmood** the PhD scholar of this department. Without their passionate participation and input, the validation survey could not have been successfully conducted.

Finally, I must express my very profound gratitude to my parents and to my whole family members including my sister **Rida Farooq**, brother **Shahmeer Hassan**, my dearest cousin **Tayyaba Chaudhry** and specially my aunt **Fehmeeda Azam** for providing me with unfailing support and continuous encouragement throughout my years of study and through the process of researching and writing this thesis. This accomplishment would not have been possible without them. Thank you.

Finally, I offer my regards and blessings to every body who was important to the successful realization of thesis, as well as expressing my apology that I could not mention all of them.

Ayesha Farooq

Contents

List of Figures

List of Tables

Abbreviations

PDEs	**P**artial **D**ifferential **E**quations
BDM	**B**rinkman **e**xtended **D**arcy **M**odel
BFDM	**B**rinkman **F**orchheimer **D**arcy **M**odel

Nomenclature

c_p	specific heat at constant pressure (JK$g^{-1}K^{-1}$)
k	thermal conductivity of fluid ($Wm^{-1}K^{-1}$)
$Nu_{\mathbf{x}}$	**l**ocal Nusselt number
$Nu_{\mathbf{avg}}$	**a**verage Nusselt number
Pr	Prandtl number (ν_f / α_f)
Ri	Richardson number (Gr / Re^2)
Gr	Grashof number (gβ_f(T_H - T_C)H^2 / ν_f^2)
Re	Reynolds number ($\rho_f u_o$H / μ_f)
Da	Darcy number (κ / H^2)
T	temperature (K)
H	cavity height(m)
l	channel length
L	cavity length
w	channel height
x, y	cartesian cordinates
X, Y	dimensionless cartesian cordinates
u, v	velocity component in x , y direction (ms^{-1})
u_0	velocity of the flow at the inlet (ms^{-1})
U, V	dimensionless velocity
p	pressure
P	dimensionless pressure

Greek Symbols

θ	dimensionless temperature
ϕ	solid volume fraction
γ	inclination angle of the channel
α	thermal diffusivity
β	thermal expansion coefficient
ρ	density (kgm^{-3})
ν	kinematic viscosity
μ	dynamic viscosity
κ	permeability of porous medium

Subscripts

f	pure fluid
nf	nanofluid
avg	average
s	solid
C	cold
H	hot

I wish to dedicate this thesis to my late mother,

NAHEEDA AZAM

She taught me to persevere and prepared me to face the challenges with faith and humility. She was constant source of inspiration to my life. Although, she is not here to give me strength and support but I always feel her presence that used to urge me to strive to achieve my goals in life.

And My father

CH. M. FAROOQ

Who always had confidence in me and offered me encouragement and support in all my endeavors.

Chapter 1

Introduction

The term mixed convection is basically induced by the process of heat transfer in fluids where both forced and natural convection mechanisms are discussed simultaneously. Mixed convection flow and heat transfer in open cavities have received great interest in recent years and tremendously seeking an importance due to wide range of engineering applications such as nuclear reactors, crystal growth, heat exchangers, solar collectors as discussed in [1].

The study in open U-shaped cavities have been discussed by increasing and decreasing effects of natural and mixed convection. Manca *et al.* [1] reviewed numerically about mixed convection fluid flow in two-dimensional horizontal open cavity with the heated wall. The computational study showed the maximum decrease in temperature values with an the Reynolds number and the Richardson number increases. A similar simulation was also conducted by Manca *et al.* [2] in 2006 in mixed convection left heated wall in an open cavity. They examined the maximum increase in temperature as the Reynolds number and Richardson number decreases. Later on, in 2008 Manca *et al.* [3] again numerically studied an investigation of opposing mixed convection in a channel with an open cavity. The parameters used in this investigation are Reynolds number and Richardson number. After further studying, the influence of Rayleigh number, Reynolds number and Hartmann number are also involved on two-dimensional governing equations by using Galerkin weighted residual by finite element technique by Rahman *et al.* [4]. Variation of all parameters such as by increasing Re and Ra shows the increases in heat transfer and Nu_{avg} decreases by increasing Ha. A numerical study was conducted by Leong *et al.* [5] on mixed convection with an open cavity in a horizontal channel considering forced convection flow. They studied for a wide range of governing parameters, i.e., Reynolds number (Re) and Grashof number. So in mixed convective region, heat transfer rate becomes lesser. A similar study has been carried out to investigate the effects of mixed convection assisting incompressible laminar flow by Stiriba [6]. It is founded

that by increasing the Grashof number and Reynolds numbers, Nusselt number Nu_{avg} increases slightly and at $Re = 100$ and $Gr \leq 10^{-1}$, the average Nusselt number remains the same. Another study was done in 2013 by Stiriba *et al.* [7] shows the experimental investigation of laminar flow in an open cavity with heating from below similar in above. From numerical study, it is observed that by increasing the Richardson number, buoyancy forces become stronger and fluid present in the cavity moves towards left while recirculating flow in the cavity is shown for high Reynolds number Re. Alinia *et al.* [8] presented two sided inclined lid driven cavity containing of water and SiO_2. Behavior of different inclination angle (θ) are discussed by varying the parameters as Ri with fixed Grashof number = 10^4. Computational results are derived in two-dimensional inclined square enclosed cavity with different θ fixing Prandtl number with base fluid concentration of nanoparticles in volume. Observing by streamlines, it is clearly seen that at low Ri, strong circulation is maintained in cavity and by increasing Ri buoyancy acts in opposite sides with $\phi = 0$ and 0.08. For Ri = 10, heat transfer rate Nu_{avg} does not show a dominant effect.

A comprehensive study was made by Nada and Chamkha [9] in lid driven inclined square with nanofluid. The two-dimensional nanofluid is water-based containing Al_2O_3 nanoparticles. As the dimensionless equations are analyzed by varying the parameters Gr, ϕ and Ri. It is observed that increasing the volume of nanoparticles and inclination angle, average Nusselt number increases. In the similar way, Sharif [10] reported the numerical presentation of laminar mixed convection in a driven cavity with hot moving lid on top wall while the bottom wall is at cold temperature. Computations are analyzed for Rayleigh number, fixing Reynolds number, inclination angle $\gamma$with Prandtl number $Pr = 6$. Mixed convection and natural convection results are simulated numerically. Thus, the average Nusselt number increases simultaneously with the inclination angle for mixed convection while it increases more rapidly having the case for natural convection. In this view, Mehrez discussed different types of nanoparticles (Al_2O_3, Cu, TiO_2 and C_uO) in Mehrez *et al.* [11] in 2013. Varying various parameters like Reynolds number, Richardson number and nanoparticles. It was observed that enhancement of heat transfer rate in Cu-water nanoparticles is high as compared to Al_2O_3water. Conclusions were approximately same that Nusselt number Nu increases with the increment in Re and also by increased intensity of solid volume fraction ϕ. Later on, entropy generation and mixed convection was carried out by Mehrez *et al.* [12] in horizontal channel of an open cavity with bottom heated wall while other walls were insulated using same technique as discussed above (Finite volume method). So enhancement in an average Nusselt number affects by the increase in parameters Re and Ri.

Mixed convection and heat transfer are of extendible interest in science and engineering fields. In recent years, technology of nanofluid has emerged a new enhanced heat transfer application. Moreover, after studying the various induction of copper particles in fluid flow

inside the geometry with inclined cavity shows the enhancement of heat transfer rate with increment in the solid volume fraction ϕ. An attracted interest is introduced in recent few decades where heat transfer exchange is studied in porous medium with the implementation of different models showing conclusions in various geometries.

Khanefar and Chamka [13] numerically studied the unsteady mixed convection in a lid driven enclosure with in porous media. Applying Brinkman-extended Darcy model, the average Nusselt number is affected. He found that by increasing the Da, heat transfer rate increases and also by increasing Da and decreasing Ri, again Nu increases. A similar observation is presented with unsteady flow and occupies the same conclusions in Rahman *et al.* [14] where (BDM) model is used with the induction of induced semi-circular heaters at the bottom wall of lid driven cavity. Vishnuvardhanarao and Das [15] has performed an experiment on two dimensional with two sided lid driven parallel in square cavity filled with saturated fluid porous medium. In this observation, Grashof number effect is more dominant when Gr is increased and heat transfer through lid enclosure is increased when porosity in enclosure is decreases. Hassan and Ismael [16] introduced the porous medium by Maxwell Brinkman model inside lid driven square cavity. The results clearly shows that as reducing the Darcy number, enhancement is seen in the heat transfer due to the existence of porous layer at two different points.

A survey on the literature has also revealed the advanced model confining porous medium is known as Brinkman Forchheimer - extended Darcy model which is the combination of BDM and BFDM. Hadim and Chen [17] concluded numerically mixed convection flow in a porous vertical channel with heat sources at the walls. With the effect of porosity, as Da decreases, Nu_{avg} increases in the vertical flow. Recently in 2016, similar model is considered for porous enclosed geometry with Cu nanoparticles in the fluid observed by Sureshkumar and Muthtamilselvan [18]. Extended BFDM is applied. Conclusions are made to find the effect of heat transfer rate. Nu_{avg} increases with high Darcy number where as porosity is fixed because higher value of Darcy number increases the flow conductance with the permeability in the fluid. Furthermore, decreasing the Richardson number, higher heat transfer rate is seen in the enclosure. Nagarajan and Akbar [19] studied the numerical modeling of mixed convection with Cu- nanoparticles in square filled enclosure bisecting the moving plate kept at the middle. Slight change in parameters does not effects the Nu_{avg}, as increment in the Darcy number increases the heat transfer rate. Significant comparison is found in Kumar *et al.* [20] between BDM and BFDM. The results depicted in this model are same as above but effect of Darcy number, Grashof number and Richardson number makes different changes in both cases. In the absence of inertial term shown in BFDM, BDM obtains increasing values of Nu_{avg}. Jeng and Tzeng. [21] explored the study including aluminium foams in fluid saturated porous media. Thus, due to greater porosity effect on momentum and energy equation,

higher heat transfer rate concludes for low Darcy number. Similarly, Kumar and Gupta in ([22],[23]) examined the heat transfer and flow in non- darcy porous media. Furthermore, Chen *et al.* [24] also discussed the CuO nanoparticles in fluid flow conducted in small tube. Nasrin and Alim [25] studied the numerical analysis of forced flow in horizontal open channel with cavity showing the induction of porous medium having TiO_2 nanoparticles. Increment in TiO_2 nanoparticles tremendously increases the heat transfer rate. So, average Nusselt number Nu_{avg} increases for low values of Darcy number.

1.1 Thesis Contributions

The main demonstration of the present study is to perform the numerical analysis in the mixed convection flow of nanofluid in an inclined open cavity and to examine the effect of different parameters. Our problem consists of four coupled nonlinear partial differential equations that are solved by using Galerkin finite element technique. Graphical results are presented and discussed quantitatively to illustrate the solution.

1.2 Outline of the dissertation

We divided this thesis into five chapters:

Chapter 1 describes the brief introduction of the present work.

Chapter 2 contains some important definitions, concepts and laws that are helpful in understanding the work in third and fourth chapter.

Chapter 3 presents the numerical observation of flow in two-dimensional, incompressible, laminar and steady flow .

Chapter 4 extends the flow analysis of Chapter 3 of nanofluid. This chapter consists of general introduction, mathematical formulation, numerical solution and results. Non-linear PDE's involving mass and momentum. Finite element technique is used to solve this model. Numerical values are considered by different ranges of Reynolds number Re, Grashof number Gr, Richardson number Ri, inclination angle γ and volume fraction ϕ where Nusselt number has also been computed and discussed in this work

Chapter 5 completely summarizes the work and concludes the dissertation.

Chapter 2

Fundamental Concepts and Governing Equations

2.1 Basic Terminologies

Definition 2.1.1. (Fluid)

A fluid is a substance that continuously deforms under an applied shear stress, i.e., changes regularly under the effect of shear stress. It is a material that has no fixed shape and modify easily to external pressure which includes gas, liquid and plasmas to some extent.

Definition 2.1.2. (Fluid mechanics)

Fluid mechanics is the branch of physics and engineering that deal with the study of flow and forces within the fluids. It deals with different characteristics of fluids. It is mainly divided into two main branches which are fluid dynamics and fluid statics.

Definition 2.1.3. (Fluid dynamics)

Fluid dynamics is the branch of an applied science which is concerned with the movement of fluid, i.e., liquid or gases in the state of motion such as in air or gas called as aerodynamics and in liquid motion, known as hydrodynamics.

Definition 2.1.4. (Fluid statics)

Fluid statics is the branch of fluid mechanics which studies the fluid at rest and also embraces the characteristics of fluid under the condition of rest means statics condition is known as fluid statics.

Definition 2.1.5. (Pressure)

The continuous physical force exerted on the unit area of surface is said to be pressure. It is expressed by P and mathematically, it can be written as

$$P = \frac{F}{A}, \tag{2.1}$$

where F and A denote the applied physical force and area of the surface, respectively.

Definition 2.1.6. (Density)

Density is defined as mass per unit volume. It is represented by Greek letter ρ and mathematically, it is defined as

$$\rho = \frac{m}{V}, \tag{2.2}$$

where m and V are the mass and volume of the substance, respectively.

Definition 2.1.7. (Viscosity)

The quantity that expresses the magnitude due to internal friction in the state of thick and semi-fluid, as measured in unit area by the force when different forces are acting on it. It is known by μ and mathematically, it can be written as

$$\mu = \frac{\text{shear stress}}{\text{shear strain}}.$$

Definition 2.1.8. (Dynamic viscosity)

Dynamic viscosity is the quantity measuring the force required to overcome internal resistance in the fluid.

Definition 2.1.9. (Kinematic viscosity)

A quantity representing the ratio between the dynamic viscosity and density. Symbolically, it can be written as ν and mathematically, it is expressed by

$$\nu = \frac{\mu}{\rho}, \tag{2.3}$$

where μ denotes dynamic viscosity and ρ denotes density respectively.

Definition 2.1.10. (Nanofluid)

Another class of fluid that contains nanometer-sized particles known as nanoparticles, typically made up of oxides, metals, carbon nanotubes or carbides. These are the fluids in which nanoparticles are suspended in the base fluid.

Definition 2.1.11. (Nanoparticles)

The nanoparticles used in nanofluids are typically made of metals, oxides, copper, carbides or carbon nanotubes.

Definition 2.1.12. (Darcy number)

The Darcy number Da represents the effect of the permeability of medium according to its cross sectional area.

$$Da = \frac{\kappa}{H^2}, \tag{2.4}$$

where κ shows the permeability of porus medium and H is the length of prescribed geometry. It was first introduced by Henry Darcy. It is transformed by the non dimensionalizing the differential form of Darcy's law.

Definition 2.1.13. (Porous medium)

A material containing the pores in it is called porous material or a porous medium. Pores are usually filled with fluid, i.e., liquid or gases. A porous medium is often considered by its porosity. Many natural materials such as soil, rocks (e.g., aquifers, petroleum, zeo-lites), biological tissues (e.g., wood, bones, cork) and hand made substances such as ceramics and cements can be characterized as porous media.

2.2 Classification of Fluids

Definition 2.2.1. (Ideal fluid)

An ideal fluid is defined as containing the null viscosity constant ($\mu = 0$) and density. It treats as incompressible and requires no viscosity due to non-availability of shear force. It is

also known as inviscid fluid.

$$\tau_{yx} = \mu \left(\frac{du}{dy} \right). \tag{2.5}$$

where τ_{yx} is shear stress and $\mu = 0$.

Definition 2.2.2. (Real fluid)

The fluid containing some viscosity effect is said to be real or viscous fluid having ($\mu > 0$), viscosity in reality where the motion present in the fluid is known as viscous flow.

Definition 2.2.3. (Newtonian fluid)

A fluid in which the viscous stresses that arises from its flow are linearly proportional to the strain, i.e., the rate of change of its deformation, as shear stress and the rate of deformation are directly proportional to each other is called as Newtonian fluids. In other words, the fluid which obeys the Newton's law of viscosity are called Newtonian fluids. Mathematically, defined as

$$\tau = \mu \frac{du}{dy}, \tag{2.6}$$

where τ is the shear stress, u denotes the x-component of velocity and μ denotes dynamic viscosity. The common examples of Newtonian fluids are air, oxygen gas, alcohol, milk, glycerol and silicone/thin motor oil etc.

Definition 2.2.4. (Non-Newtonian fluid)

When shear stress is not directly proportional to the velocity gradient are defined as Non-Newtonian fluid. In other words, the fluid which does not obey the Newton's law of viscosity is said to be Non-Newtonian fluids. Mathematically, it can be expressed as

$$\tau_{xy} \propto \left(\frac{du}{dy} \right)^m, \ m \neq 1 \tag{2.7}$$

$$\tau_{xy} = \nu \left(\frac{du}{dy} \right), \ \nu = j \left(\frac{du}{dy} \right)^{m-1},$$

where ν denotes the apparent viscosity, m is the index of flow performance and the constancy index is j. Note that for $m = 1$, above equation reduces to the Newton's law of viscosity. Examples of non-Newtonian fluids are toothpaste, ketchup, starch suspensions, custard, maizena, shampoo, paint and blood etc.

2.3 Types of Flows

Definition 2.3.1. (Flow)

An object that mostly involves the steady movement of flow leading to an unbounded distortion. Several types of flow are as follow:

Definition 2.3.2. (Laminar flow)

In fluid dynamics, laminar flow occurs when a flow is in parallel layers/closed channel or flat plates with no interruption between the plates. Typically, each particle has a definite path and the particles of the path in the fluid do not cross each other. Rising of smoke is an example of laminar flow.

Definition 2.3.3. (Turbulent flow)

When fluid undergoes irregular fluctuations or flowing faster, this type of fluid (liquid or gas) is called turbulent flow. Turbulent flow which moves randomly in any direction and has no definite path and can't be handled easily. It undergoes changes both in magnitude and direction.

Definition 2.3.4. (Steady flow)

The flow that does not changes with respect to time is called steady flow.
Mathematically, it can be written as

$$\frac{d\eta^*}{dt} = 0, \tag{2.8}$$

where η^* is fluid property.

Definition 2.3.5. (Unsteady flow)

The flow that continuously changes with respect to time, is expressed as unsteady flow.
Mathematically, it can be written as

$$\frac{d\eta^*}{dt} \neq 0, \tag{2.9}$$

where η^* is fluid property.

Definition 2.3.6. (Compressible flow)

A compressible flow is the branch of fluid mechanics which varies significant changes during the fluid flow used in high-speed jet engines, aircraft, rocket motors also in high-speed usage

in a planetary atmosphere, gas pipelines and in commercial fields. Mathematically, it is expressed as

$$\rho(x, y, z, t) \neq c, \tag{2.10}$$

Definition 2.3.7. (Incompressible flow)

A type of fluid flow mechanics in which the density remains constant throughout during the flow, is called incompressible flow. Mathematically, it can be expressed by

$$\rho(x, y, z, t) = c, \tag{2.11}$$

where c is a constant.

Definition 2.3.8. (Uniform flow)

The flow defined in which velocity and hydrodynamic parameters does not changes from point to point at any given instant, having same direction as well as magnitude during the fluid motion called as uniform flow. Mathematically, it can be expressed as

$$\frac{\partial \mathbf{V}}{\partial s} = 0, \tag{2.12}$$

where $\mathbf{V}$ is the velocity and s is the displacement.

Definition 2.3.9. (Non uniform flow)

In non-uniform flow, the velocity and hydrodynamic parameters changes from one point to another point and the velocity is not same at every point of the fluid at an instant. Mathematically, it is written as

$$\frac{\partial \mathbf{V}}{\partial s} \neq 0, \tag{2.13}$$

where $\mathbf{V}$ is the velocity and s is the displacement in any direction.

Definition 2.3.10. (External flow)

The flow for which the fluid is not bounded by the solid surface. Water flow in rivers and oceans are the examples of external flow.

Definition 2.3.11. (Internal flow)

The flow is bounded and confined by the solid surface and convenient geometry for cooling and heating fluids used in the energy is called as internal flow. The example of the internal flow are the flow of a pipe or glass.

2.4 Heat Transfer Mechanism and related properties

Definition 2.4.1. (Conduction)

The flow of heat transfer through liquid or solid with rapid vibration between neighboring molecules and atoms. In other words when free electrons moves from one atom to another is known to be conduction. Mathematically, it can be written as

$$q = -k\mathrm{A}\left(\frac{\Delta T}{\Delta n}\right), \tag{2.14}$$

where k denotes the constant of the thermal conductivity and $\frac{\Delta T}{\Delta n}$ denotes gradient of temperature respectively.

Definition 2.4.2. (Convection)

The process in which fluid is forced by external processes and when thermal energy expands in gravitational fields by the interaction of buoyancy forces then it is called convection. Gases and liquid are the examples of convection fluid. Mathematically, it is expressed as

$$q = h\mathrm{A}(T_s - T_\infty), \tag{2.15}$$

where h, A, T_s and T_∞ expresses the heat transfer coefficient, the area, the temperature of the surface. It is further simplified into following three categories.

Definition 2.4.3. (Force convection)

Force convection is a type of communication in which motion of fluid is generated by an outer source (like a fan, pump etc.) is known as force convection. It is also used in machines, air conditioning, central heating and in many other turbines.

Definition 2.4.4. (Natural convection)

When motion of fluid is not generated by an independent source then it is said to be natural convection or called free convection. Simplifying more, it occurs due to the temperature

gradient differences having effect on the density. Natural convection can only exists in gravitational field.

Definition 2.4.5. (Mixed convection)

A flow which is simultaneously characterized by both forced and free convection processes and acting simultaneously. Mixed convection is always realized when small number of velocities are characterized on cooling and heating of walls.

Definition 2.4.6. (Thermal conductivity)

The property of a material related to its capacity to conduct the heat is known as thermal conductivity. Fourier law of conduction which relates the rate of heat transfer by conduction to the temperature gradient is

$$\frac{dQ}{dt} = -k\mathrm{A}\frac{dT}{dx}, \tag{2.16}$$

where A, k, $\frac{dQ}{dt}$, $\frac{dT}{dx}$ is the area, thermal conductivity, the rate of heat transfer and the temperature gradient respectively. With the increase of temperature, thermal conductivity of most liquids decreases except water. The SI unit of thermal conductivity is $\frac{Kg.m}{s^3}$ and its dimension is $[\frac{ML}{T^3}]$.

Definition 2.4.7. (Thermal diffusivity)

Thermal diffusivity is material's property for characterizing unsteady heat conduction (k) of a substance to specific heat at constant pressure (c_p) and density (ρ). It measures the ability of a substance to conduct thermal energy relative to its ability.
Mathematically, it can be written as

$$\alpha = \frac{k}{\rho c_p}. \tag{2.17}$$

2.5 Dimensionless numbers

Definition 2.5.1. (Nusselt number)

Nusselt number (Nu_{avg}) is a dimensionless parameter used in numerical analysis of heat transfer at the boundary between a solid body and a moving fluid. Nusselt number is close to conduction and convection of same magnitude and is also characterized as "laminar flow". It was firstly introduced by the German mathematician Nusselt, expressed by Nu is the dimensionless number. Mathematically, Nusselt number is denoted by

$$Nu_x = \frac{k_{nf}}{k_f}\left(\frac{\partial\theta}{\partial X}\right), \tag{2.18}$$

where k_{nf} presents the thermal conductivity of nanofluid and k_f shows thermal conductivity of fluid. Similarly, average Nusselt number is induced by integrating the local Nusselt number which shows the overall heat transfer exchange present in the cavity. It is defined as follow

$$Nu_{\text{avg}} = \int Nu dY, \tag{2.19}$$

Definition 2.5.2. (Prandtl number)

The ratio of the kinematic diffusivity/momentum diffusivity to the thermal diffusivity is known to be the Prandtl number, named by the Ludwig Prandtl a German physicist. It is expressed by Pr and mathematically it can be written as

$$Pr = \frac{\rho_f (C_p)_f}{k_f}, \tag{2.20}$$

where ρ_f expresses the density fluid and C_p denotes the specific heat and k_f shows thermal conductivity of fluid respectively. It superivises temperature function and the relative thickness of momentum. Physical significance of Prandtl number is that it gives the thermal boundary layer and velocity thickness. Pr is approximately constant for gases over a wide range of pressure and temperature.

Definition 2.5.3. (Grashof number)

The Grashof number introduced by German engineer Franz Grashof as a dimensionless parameter that expresses the relationship between viscous force and buoyancy force acting on a fluid is called Grashof number. It frequently expresses in the study involving the free convection or natural convection. Symbolically it can be denoted as Gr and mathematically it can be defined as

$$Gr = \frac{g\beta_f (T_H - T_C) H^3}{\nu_f^2}, \tag{2.21}$$

where, β_f denotes coefficient of thermal expansion, g represents the gravitational acceleration, T_H, T_C shows the surface temperature, H, denotes the height of cavity, ν denotes the kinematic viscosity.

Definition 2.5.4. (Reynolds number)

The branch of fluid mechanics used to indicate behavior of fluid in the boundary layer and have a relationship between inertial forces to the viscous forces. The Reynolds number can be predicted for several different situations where a fluid surface is in relative motion. It is denoted by Re and mathematically it can be written as

$$Re = \frac{\rho_f u_o H}{\mu_f}, \tag{2.22}$$

where μ represents dynamic viscosity, u_o denotes the flow velocity of the inlet.

Definition 2.5.5. (Richardson number)

The Richardson number was first introduced by Lewis Fry Richardson as a dimensionless parameter that expresses the relationship of buoyancy term with flow shear term. It is denoted by Ri and mathematically it can be written as

$$Ri = \frac{Gr}{Re^2}, \tag{2.23}$$

where Gr represents the Grashof number and Re is the Reynolds number. If the Richardson number is less than unity then buoyancy becomes unimportant in the fluid flow. As Richardson number is used in the importance of weather forecast and in the investigation of density, lakes oceans and reservoirs.

2.6 Basic equations

Definition 2.6.1. (Continuity Equation)

Continuity equation is derived from the law of conservation of mass and mathematically, it is expressed by

$$\frac{\partial \rho}{\partial t} + \nabla.(\rho \mathbf{V}) = 0, \tag{2.24}$$

where t is the time. If fluid is an incompressible then the continuity equation is expressed by

$$(\nabla \ . \ \mathbf{V}) = 0. \tag{2.25}$$

Definition 2.6.2. (Law of conservation of momentum)

Each particle of fluid obeys Newtons second law of motion which is at rest or in steady state or accelerated motion. This law states that the combination of all applied external forces acting on a body is equal to the time rate of change of linear momentum of the body. In vector notation this law can be written as

$$\rho \frac{d\mathbf{V}}{dt} = \text{div}T + \rho b, \tag{2.26}$$

for Navier-Stokes equation

$$T = -pI + \mu A_1, \tag{2.27}$$

where A_1 is the tensor and first time it was produced by Rivlin-Erickson.

$$A_1 = \text{grad}\mathbf{V} + (\text{grad}\mathbf{V})^t, \tag{2.28}$$

In the above equations, $\frac{d}{dt}$ denote material time derivative or total derivative, ρ denote density, $\mathbf{V}$ denote velocity field, T the Cauchy stress tensor, b the body forces, p the pressure, μ the dynamic viscosity.
The Cauchy stress tensor is expressed in the matrix form

$$T = \begin{pmatrix} \sigma_{xx} & \tau_{yx} & \tau_{zx} \\ \tau_{xy} & \sigma_{yy} & \tau_{zy} \\ \tau_{xz} & \tau_{yz} & \sigma_{zz} \end{pmatrix}, \tag{2.29}$$

where σ_{xx}, σ_{yy} and σ_{zz} are normal stresses, others wise the shear stresses. For two-dimensional flow, we have $V = [u(x, y, 0), v(x, y, 0), 0]$ and thus

$$\text{grad}V = \begin{pmatrix} \frac{\partial u}{\partial x} & \frac{\partial u}{\partial y} & 0 \\ \frac{\partial v}{\partial x} & \frac{\partial v}{\partial y} & 0 \\ 0 & 0 & 0 \end{pmatrix}. \tag{2.30}$$

$$\frac{\partial u}{\partial t} + u\frac{\partial u}{\partial x} + v\frac{\partial v}{\partial y} = -\frac{1}{\rho}\frac{\partial p}{\partial y} + \nu\left(\frac{\partial^2 u}{\partial x^2} + \frac{\partial^2 u}{\partial y^2}\right), \tag{2.31}$$

Similarly, we repeat the above process for Y component as follows:

$$\frac{\partial v}{\partial t} + u\frac{\partial v}{\partial x} + v\frac{\partial v}{\partial y} = -\frac{1}{\rho}\frac{\partial p}{\partial y} + \nu\left(\frac{\partial^2 v}{\partial x^2} + \frac{\partial^2 v}{\partial y^2}\right). \tag{2.32}$$

Definition 2.6.3. (Energy Equation)

The energy equation for the fluid is

$$\rho C_p\left(\frac{\partial}{\partial t} + \mathbf{V}\nabla\right)T = k\nabla^2 T + \tau L + \rho C_p\left[D_B\nabla C.\nabla T + \frac{DT}{Tm}\nabla T\right], \tag{2.33}$$

where $(C_p)_f$ denotes the specific heat of the basic fluid, $(C_p)_s$ the specific heat of the material, ρ_f the density of basic fluid, L denote the rate of strain tensor and T the temperature of the fluid, D_B the Brownian motion coefficient and D_T the temperature diffusion coefficient and T_m denote the mean temperature. The expression for Cauchy stress tensor τ for viscous incompressible fluid is expressed by

$$\tau = -pI + \mu A_1, \tag{2.34}$$

where A_1 is the tensor, p the pressure and μ the dynamic viscosity.

$$A_1 = \text{grad}\mathbf{V} + (\text{grad}\mathbf{V})^t, \tag{2.35}$$

where t represents transpose of the matrix for two dimensional field velocity of the fluid, T the stain tensor and can be written as

$$T = \begin{pmatrix} \sigma_{xx} & \tau_{yx} & \tau_{zx} \\ \tau_{xy} & \sigma_{yy} & \tau_{zy} \\ \tau_{xz} & \tau_{yz} & \sigma_{zz} \end{pmatrix}. \tag{2.36}$$

2.7 Finite Element Method

Finite Element Method is used as a numerical technique for analyzing the nonlinear partial differential equations. It mainly assembles in finding the approximate solutions to boundary value problems for partial differential equations. It is also called finite element analysis (FEA). FEM subdivides a large domain into collection of smaller, simpler domain using mesh levels called finite elements. Basically this method is an easy presentation of whole solution.[26]

Definition 2.7.1. (Galerkin Finite Element Method)

Explaining the observation experimentally, the Galerkin method is used in Finite element scheme. Final calculations are easily originated by combining the local system into global system with set of elements. Moreover, Galerkin method is also compatible for linear and non-linear coupled partial differential equations. For convergence, both Newton Iteration Method and Jacobi Method are applicable through finite element coding.[26]

- Write the strong formulation of the governing equations.
- Multiply both sides of the governing equations by weighted function also called test function w with given test space W where w ϵ W.
- Use rules of integration by parts to distribute the higher order of differentiation between the unknown variable U and the test function w.
- Evaluate the boundary integral values by the induction of weighted function to satisfy the homogeneous form of the essential boundary conditions and also the unknown variables are used to satisfy the natural boundary conditions called as Variational formulation.

- Generate mesh which divides the entire domain into non-overlapping elements depending upon the dimensions used for present problem.
- Approximate the infinite dimensional trial space U, V and test space W by finite dimensional spaces U_h, V_h and W_h, respectively where U_h(finite dimensional space) $\subset$ U (solution space).
- Choose basis functions ϕ_1,ϕ_2,...ϕ_N of w_h, so that every test functions $w_h \epsilon W_h$ can be written as $w_h = \sum_{i=1}^{N} w_i\varphi_i \in W_h$,.
- Find $u_h \epsilon U_h$ such that $a(u_h, w_h) = b(w_h) \quad \forall\ w_h = \sum_{i=1}^{N} w_i\varphi_i \in W_h$,

$$\Rightarrow a(u_h, \varphi_i) = b(\varphi_i), \quad \text{where } (i = 1, 2, 3, \cdots, N).$$

Substituting $u_h = \sum_{j=1}^{N} u_j\varphi_j$, in above equation gives a linear system, that is,

$$a\Big(\sum_{j=1}^{N} u_j\varphi_j, \varphi_i\Big) = b(\varphi_i) \quad \text{for } i, j = (1, 2, \cdots, N).$$

$$\Rightarrow \sum_{j=1}^{N} a(\varphi_j, \varphi_i)u_j = b(\varphi_i) \quad \text{for } i, j = (1, 2, \cdots, N).$$

where u_j are the solution values at the points. Separating into linear b(w) and bilinear form a(u, w).

- (AU = B) is transformed which assembles the algebraic equations by varying i and j in row and column wise.

2.7.1 Advantages

Some of the basic features of Finite Element Method given below are discussed in [27]

- The most useful feature of this method is to show Accurate presentation of complexed geometry.
- Divides the domain into a collection of sub-domains where each represented by a set of element equations to the present problem.
- Systematically, recombines the set of element equations into global system by local system with easy representation.

Chapter 3

Numerical simulation of mixed convective nanofluid flow in an inclined channel with cavity

In this chapter, we will analyze the numerical study of uniform left heated wall of the open cavity and time independent mixed convection assisting flow of Cu-water nanofluid in an inclined open cavity by the Finite element method. By using transformation, the system of four nonlinear coupled partial differential equations such as continuity, momentum and energy equation [1] are converted into dimensionless equations and analyzed by the Galerkin weighted residual method. In this chapter we have discussed complete review of the paper in Mehrez *et al.* [28].

3.1 Problem Formulation

The fluid flow and the heat transfer in a two dimensional inclined open cavity of length L is considered, as shown in the schematic diagram of Figure 3.1. It considers the effect of invoking different inclination angles in a channel with flowing nanofluid of Cu-water on mixed convection heat transfer. As the left side of the wall has uniform heat distribution T_H and cold flow enters through the left side of the channel at constant temperature T_C. The remaining walls of cavity are adiabatic. The size and shape of solid particles are characterized as uniform and nanoparticles and basefluid are considered in thermal equilibrium. Demonstrative effect is shown on fluid flow by considering different Reynolds numbers. The impact of governing equations are analyzed by streamlines, isotherms and average Nusselt numbers. Taking in account the above assumptions and in consideration of Boussinesq approximation, the

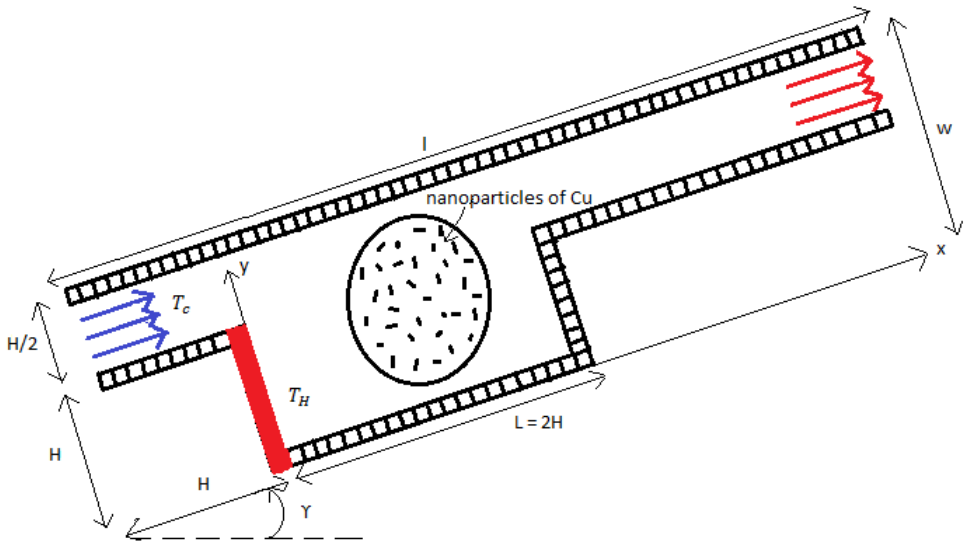

FIGURE 3.1: Physical model of schematic diagram.

dimensional equations are as follow

Continuity equation

$$\frac{\partial u}{\partial x}+\frac{\partial v}{\partial y}=0, \tag{3.1}$$

x - Momentum equation

$$\rho_{nf}\left(u\frac{\partial u}{\partial x}+v\frac{\partial u}{\partial y}\right)=-\frac{\partial p}{\partial x}+\mu_{nf}\left(\frac{\partial^2 u}{\partial x^2}+\frac{\partial^2 u}{\partial y^2}\right)+(\rho\beta)_{nf}g(T-T_c)(\sin\gamma), \tag{3.2}$$

y - Momentum equation

$$\rho_{nf}\left(u\frac{\partial v}{\partial x}+v\frac{\partial v}{\partial y}\right)=-\frac{\partial p}{\partial y}+\mu_{nf}\left(\frac{\partial^2 v}{\partial x^2}+\frac{\partial^2 v}{\partial y^2}\right)+(\rho\beta)_{nf}g(T-T_c)(\cos\gamma), \tag{3.3}$$

Energy equation

$$u\frac{\partial T}{\partial x}+v\frac{\partial T}{\partial y}=\frac{\alpha_{nf}}{\alpha_f}\frac{1}{RePr}\left(\frac{\partial^2 T}{\partial x^2}+\frac{\partial^2 T}{\partial y^2}\right). \tag{3.4}$$

Here, u, v express the component of velocity along x-direction and y-direction, respectively, p denotes the pressure, T shows the temperature and γ expresses the inclination angle of the channel cavity in the horizontal direction. ϕ expresses base fluid with the contribution of nanoparticles of copper. .

Property	$\rho(kgm^{-3})$	$C_p(J/kg^{-1}K^{-1})$	$k(Wm^{-1}K^{-1})$	$\beta 10^{-5}(K^{-1})$
Water	997.1	4179	0.613	21
Copper(Cu)	8933	385	400	1.67

TABLE 3.1: Thermo-physical properties of water and Cu-nanofluid[11].

3.2 Non-dimensionlized Form of the Governing Equations:

To make the above governing equations Eqs. (3.1) - (3.4) dimensionless, we initialize the following dimensionless parameters involved are:

$$Re = \frac{\rho_f u_o H}{\mu_f}, \qquad Pr = \frac{\rho_f (C_p)_f}{K_f}, \qquad Ri = \frac{Gr}{Re^2} = \frac{g\beta_f (T_H - T_C)H}{u_o^2}, \qquad Gr = \frac{g\beta_f (T_H - T_C)H^2}{\nu_f^2}$$

As non-dimensional variables are defined as:

$$X = \frac{x}{H}, \qquad Y = \frac{y}{H}, \qquad U = \frac{u}{u_o}, \qquad V = \frac{v}{u_o}, \qquad P = \frac{p}{\rho_{nf} u_o^2}, \qquad \theta = \frac{(T - T_C)}{(T_H - T_C)}.$$

By using these dimensionless parameters and variables, the above governing equations are reduced in this way given below

$$\frac{\partial U}{\partial X} + \frac{\partial V}{\partial Y} = 0, \tag{3.5}$$

$$U\frac{\partial U}{\partial X} + V\frac{\partial U}{\partial Y} = -\frac{\partial P}{\partial X} + \frac{1}{Re}\frac{\rho_f}{\rho_{nf}}\frac{1}{(1-\phi)^{2.5}}\left(\frac{\partial^2 U}{\partial X^2} + \frac{\partial^2 U}{\partial Y^2}\right) + Ri\frac{\rho_f}{\rho_{nf}}\left(1 - \phi + \frac{\rho_s \beta_s \phi}{\rho_f \beta_f}\right)(\sin\gamma)\theta, \tag{3.6}$$

$$U\frac{\partial V}{\partial X} + V\frac{\partial V}{\partial Y} = -\frac{\partial P}{\partial Y} + \frac{1}{Re}\frac{\rho_f}{\rho_{nf}}\frac{1}{(1-\phi)^{2.5}}\left(\frac{\partial^2 V}{\partial X^2} + \frac{\partial^2 V}{\partial Y^2}\right) + Ri\frac{\rho_f}{\rho_{nf}}\left(1 - \phi + \frac{\rho_s \beta_s \phi}{\rho_f \beta_f}\right)(\cos\gamma)\theta, \tag{3.7}$$

$$U\frac{\partial \theta}{\partial X} + V\frac{\partial \theta}{\partial Y} = \frac{\alpha_{nf}}{\alpha_f}\frac{1}{RePr}\left(\frac{\partial^2 \theta}{\partial X^2} + \frac{\partial^2 \theta}{\partial Y^2}\right). \tag{3.8}$$

The dimensionless equations are subjected to dimensionless boundary conditions for the present problems that are given by

Nanofluid properties	Expressed model
Density	$\rho_{nf} = (1-\phi)\rho_f + \phi\rho_s$
Thermal diffusivity	$\alpha_{nf} = \frac{k_{nf}}{(\rho C_p)_{nf}}$
Heat capacitance	$(\rho C_p)_{nf} = (1-\phi)(\rho C_p)_f + \phi(\rho C_p)_s$
Dynamic viscosity	$\mu_{nf} = \frac{\mu_f}{(1-\phi)^{2.5}}$
Thermal expansion coefficient	$(\rho\beta)_{nf} = (1-\phi)\rho_f\beta_f + \phi\rho_s\beta_s$

TABLE 3.2: Implemented formulae for the nanofluid properties[18].

- On the inlet side of the channel:

$$U = 1, \quad V = 0, \quad \theta = 0. \tag{3.9}$$

- On the left wall of the cavity:

$$U = 0, \quad V = 0, \quad \theta = 1 \tag{3.10}$$

- On the rest adiabatic walls of the channel and cavity:

$$U = 0, \quad V = 0, \quad \frac{\partial\theta}{\partial Y} = 0 \text{ (for horizontal wall)} \quad \text{and} \quad \frac{\partial\theta}{\partial X} = 0 \text{ (for vertical wall).} \tag{3.11}$$

- On the outlet side of the channel:

$$\frac{\partial U}{\partial X} = 0 \quad \frac{\partial V}{\partial Y} = 0 \quad \frac{\partial\theta}{\partial X} = 0. \tag{3.12}$$

3.3 Numerical Procedure

The system of coupled non-linear partial differential Eqs. (3.5) - (3.8) together with given boundary conditions in (3.9) - (3.12) have been discretized numerically by finite element formulation together with Galerkin weighted residual technique. Non-linear PDE's shows the complete matrix defined in subjected boundary conditions. Transforming into 4 x 4 matrix with the adaptation of laplace, mass and convective matrix including non-linearity terms. The numerical procedure used to solve the governing equation for the present work that is based on the Galerkin weighted residual method of finite-dement formulation where U, V and θ are discretized by Q_2 element of 3rd order accuracy and P is discretized by P_1^{disc} element of 2nd order accuracy(see [30] for details). This technique concludes in fast convergence assurance. A quadrilateral mesh arrangement is implemented in the present task especially near the left wall to secure the rapid changes in the dependent variable by heat transfer.

3.3.1 Variational Formulation of Governing Equations

In this section, Eqs. (3.5) - (3.8) illustrate from strong form to weaker form. Multiplier method / Weak form or the Variational formulation method is an approach where the governing equations are multiplied by suitable functions known as test functions w, q and then integrated over the whole domain Ω.

$$U\frac{\partial U}{\partial X}+V\frac{\partial U}{\partial Y}=-\frac{\partial P}{\partial X}+\frac{1}{Re}\frac{\rho_f}{\rho_{nf}}\frac{1}{(1-\phi)^{2.5}}\left(\frac{\partial^2 U}{\partial X^2}+\frac{\partial^2 U}{\partial Y^2}\right)+Ri\frac{\rho_f}{\rho_{nf}}\left(1-\phi+\frac{\rho_s\beta_s\phi}{\rho_f\beta_f}\right)(\sin\gamma)\theta, \tag{3.13}$$

$$U\frac{\partial V}{\partial X}+V\frac{\partial V}{\partial Y}=-\frac{\partial P}{\partial Y}+\frac{1}{Re}\frac{\rho_f}{\rho_{nf}}\frac{1}{(1-\phi)^{2.5}}\left(\frac{\partial^2 V}{\partial X^2}+\frac{\partial^2 V}{\partial Y^2}\right)+Ri\frac{\rho_f}{\rho_{nf}}\left(1-\phi+\frac{\rho_s\beta_s\phi}{\rho_f\beta_f}\right)(\cos\gamma)\theta, \tag{3.14}$$

$$\frac{\partial U}{\partial X}+\frac{\partial V}{\partial Y}=0, \tag{3.15}$$

$$U\frac{\partial \theta}{\partial X}+V\frac{\partial \theta}{\partial Y}=\frac{\alpha_{nf}}{\alpha_f}\frac{1}{RePr}\left(\frac{\partial^2 \theta}{\partial X^2}+\frac{\partial^2 \theta}{\partial Y^2}\right). \tag{3.16}$$

Let W = $[H^1(\Omega)]^3$ shows the test spaces for u-velocity, v-velocity and temperature where Q = $L^2(\Omega)$ shows the test space for pressure. The variational form of governing equations is given as

Find (U, V, θ, P) ϵ W $\times$ Q such that

$$-\frac{\rho_f}{\rho_{nf}}\frac{1}{(1-\phi)^{2.5}}\int_\Omega\frac{1}{Re}\left(\frac{\partial^2 U}{\partial X^2}+\frac{\partial^2 U}{\partial Y^2}\right)\,w\,d\Omega+\int_\Omega\left(U\frac{\partial U}{\partial X}+V\frac{\partial U}{\partial Y}\right)\,w\,d\Omega+\int_\Omega\frac{\partial P}{\partial X}\,w\,d\Omega-Ri\frac{\rho_f}{\rho_{nf}}\left(1-\phi+\frac{\rho_s\beta_s\phi}{\rho_f\beta_f}\right)(\sin\gamma)\int_\Omega\theta\,w\,d\Omega=0, \tag{3.17}$$

$$-\frac{\rho_f}{\rho_{nf}}\frac{1}{(1-\phi)^{2.5}}\int_\Omega\frac{1}{Re}\left(\frac{\partial^2 V}{\partial X^2}+\frac{\partial^2 V}{\partial Y^2}\right)\,w\,d\Omega+\int_\Omega\left(U\frac{\partial V}{\partial X}+V\frac{\partial V}{\partial Y}\right)\,w\,d\Omega+\int_\Omega\frac{\partial P}{\partial Y}\,w\,d\Omega-Ri\frac{\rho_f}{\rho_{nf}}\left(1-\phi+\frac{\rho_s\beta_s\phi}{\rho_f\beta_f}\right)(\cos\gamma)\int_\Omega\theta\,w\,d\Omega=0, \tag{3.18}$$

$$\int_\Omega\left(\frac{\partial U}{\partial X}+\frac{\partial V}{\partial Y}\right)\,q\,d\Omega=0, \tag{3.19}$$

$$\int_\Omega\left(U\frac{\partial \theta}{\partial X}+V\frac{\partial \theta}{\partial Y}\right)\,w\,d\Omega-\frac{\alpha_{nf}}{\alpha_f}\frac{1}{RePr}\int_\Omega\left(\frac{\partial^2 \theta}{\partial X^2}+\frac{\partial^2 \theta}{\partial Y^2}\right)\,w\,d\Omega=0. \tag{3.20}$$

for all $(w,\, q)\ \epsilon$ W $\times$ Q.

By Galerkin approximation

$$\frac{\rho_f}{\rho_{nf}}\frac{1}{(1-\phi)^{2.5}}\int_\Omega \frac{1}{Re}\left(\frac{\partial U_h}{\partial X}\,\frac{\partial w_h}{\partial X}+\frac{\partial U_h}{\partial Y}\,\frac{\partial w_h}{\partial Y}\right)\,d\Omega+\int_\Omega\left(U_h\frac{\partial U_h}{\partial X}+V_h\frac{\partial U_h}{\partial Y}\right)\,w_h\,d\Omega$$
$$-Ri\frac{\rho_f}{\rho_{nf}}\left(1-\phi+\frac{\rho_s\beta_s\phi}{\rho_f\beta_f}\right)(\sin\gamma)\int_\Omega\theta_h\,w_h\,d\Omega+\int_\Omega\frac{\partial P_h}{\partial X}\,w_h\,d\Omega=0, \tag{3.21}$$

$$\frac{\rho_f}{\rho_{nf}}\frac{1}{(1-\phi)^{2.5}}\int_\Omega \frac{1}{Re}\left(\frac{\partial V_h}{\partial X}\,\frac{\partial w_h}{\partial X}+\frac{\partial V_h}{\partial Y}\,\frac{\partial w_h}{\partial Y}\right)\,d\Omega+\int_\Omega\left(U_h\frac{\partial V_h}{\partial X}+V_h\frac{\partial V_h}{\partial Y}\right)\,w_h\,d\Omega$$
$$-Ri\frac{\rho_f}{\rho_{nf}}\left(1-\phi+\frac{\rho_s\beta_s\phi}{\rho_f\beta_f}\right)(\cos\gamma)\int_\Omega\theta_h\,w_h\,d\Omega+\int_\Omega\frac{\partial P_h}{\partial Y}\,w_h\,d\Omega=0, \tag{3.22}$$

$$\int_\Omega\left(\frac{\partial U_h}{\partial X}+\frac{\partial V_h}{\partial Y}\right)\,q_h\,d\Omega=0, \tag{3.23}$$

$$\int_\Omega\left(U_h\frac{\partial\theta_h}{\partial X}+V_h\frac{\partial\theta_h}{\partial Y}\right)\,w_h\,d\Omega+\frac{\alpha_{nf}}{\alpha_f}\frac{1}{RePr}\int_\Omega\left(\frac{\partial\theta_h}{\partial X}\,\frac{\partial w_h}{\partial X}+\frac{\partial\theta_h}{\partial Y}\,\frac{\partial w_h}{\partial Y}\right)\,d\Omega=0. \tag{3.24}$$

Using FEM approximation of U_h, V_h, θ_h and P_h. In the same way converting $(w,\, q)$ test functions into basis functions as w_h, q_h.

The fully discretized system reads the following

$$\underbrace{\begin{pmatrix} a_{11}L+N(\underline{U},\underline{V}) & 0 & B_1 & b_{14}M \\ 0 & a_{22}L+N(\underline{U},\underline{V}) & B_2 & b_{24}M \\ B_1^T & B_2^T & 0 & 0 \\ 0 & 0 & 0 & a_{44}L+N(\underline{U},\underline{V}) \end{pmatrix}}_{\text{A}}\underbrace{\begin{pmatrix}\underline{U}\\ \underline{V}\\ \underline{P}\\ \underline{\theta}\end{pmatrix}}_{\text{U}}=\underbrace{\begin{pmatrix}0\\0\\0\\0\end{pmatrix}}_{\text{B}}, \tag{3.25}$$

where A is known as "block matrix", U is called "solution vector" and B is expressed as "load vector" The block matrix shows,

$$a_{11}=\frac{1}{Re}\frac{\rho_f}{\rho_{nf}}\frac{1}{(1-\phi)^{2.5}}=a_{22},$$
$$a_{44}=\frac{\alpha_{nf}}{\alpha_f}\frac{1}{RePr},$$
$$b_{14}=-Ri\frac{\rho_f}{\rho_{nf}}\left(1-\phi+\frac{\rho_s\beta_s\phi}{\rho_f\beta_f}\right)(\sin\gamma),$$
$$b_{24}=-Ri\frac{\rho_f}{\rho_{nf}}\left(1-\phi+\frac{\rho_s\beta_s\phi}{\rho_f\beta_f}\right)(\cos\gamma).$$

where L, M and N are the Laplace, mass and convective matrix. Similarly, B_1 and B_2 are the pressure matrix with their tranpose B_1^T and B_2^T.

3.4 Code Validation

A multi-dimensional steady mixed convection equations are used by finite element technique and proposed by Mehrez *et al.* [28]. The effect of grid sizes depends upon by changing different combinations of Re, γ and ϕ.

In order to formulate the mixed convection of heat transfer with Cu-water nanofluid model, validation of present computational code of steady state solution is presented by minimum stream function ψ and maximum temperature θ which is maintained in two dimensional steady state channel in inclined open cavity. In Table 3.4, an observable agreement is seen

Assisting forced flow				
Ri	Present Study	Ref. [1]	Ref. [12]	Ref. [29]
0.01	0.57623	0.576	0.575	0.577
0.1	0.54379	0.544	0.549	0.545
1	0.42042	0.42	0.426	0.422
10	0.30294	0.303	0.306	0.305
100	0.20985	0.209	—	0.211
Opposing forced flow				
Ri	Present Study	Ref. [1]		
0.01	0.62331	—		
0.1	0.62633	0.627		
1	0.61660	0.617		
10	0.23757	0.237		
100	0.13155	0.132		
Horizontal forced flow				
Ri	Present Study	Ref. [1]	Ref. [11]	
0.01	1.09456	—	—	
0.1	1.06117	1.06	1.07	
1	0.85609	0.856	0.871	
10	0.61370	0.613	0.620	
100	0.43698	0.437	—	

TABLE 3.3: Comparison of Refs. [1, 11, 12, 29] with the present results for different values of Ri.

between the present study in Mehrez *et al.* [28] with Refs. [1, 11, 12, 29] showing a slight difference. In the above table three flow cases are considered with the comparison of assisting forced flow, opposing forced and horizontal forced flow. These all flows are demonstrated in the inclined channel with cavity for $Ri = 0.01, 0.1, 1, 10, 100$.

3.5 Results and Discussion

In this section, numerical analysis of mixed convective heat transfer of Cu-water nanofluid particles in inclined open cavity is discussed. An attention is given to the effect of heat transfer rate by varying various parameters in the channel with cavity. The values of $Pr = 6.2$, $Ri = 0.04$, 1 and $Re = 100$, 500 are considered. Calculations are made by the influence of inclination angle γ ranges from 0^o to 360^o and nanoparticles of Cu-water varies from 0 (pure water) to 0.06. Grashof number $Gr = 10^4$ is considered for all values of Re.

Figure 3.2(a) illustrates the effect of streamlines for forced convection case with for $\gamma = 0^o$, 90^o, 180^o and 270^o. Strong flow strength is seen near the upper wall of the channel showing high velocity. Indeed, a large recirculating cell is developed in the cavity for all γ's. The strength of fluid flow starts decreasing at lower side of the channel with similar effect seen in the cavity. The circulation zone is induced by weaker flow magnitude which gradually grows by the increment of the angles in the cavity. At $\gamma = 180^o$, the cell induced by the flow movement moves towards the left with the slight change on the upper left side of the cavity as shear forces are seen to be more dominant in this case.

Isotherms are shown in Figure 3.2(b) for $Ri = 0.04$. Figure 3.2(b) represents the temperature gradients with different inclination angle γ. Temperature near the left hot wall of the cavity induces greater heat transfer which gradually declines in the flow away from it. The thickness of thermal boundary layer increases at $\gamma = 180^o$ and seen to be decreased for $\gamma = 270^o$. Similarly, for the case of nanofluid shown in Figure 3.3(a) and Figure 3.3(b), with the inducement of $\phi = 0.06$, the intensity in the fluid flow increases. When the density of nanoparticles become greater, the flow become more intense in the cavity. In Figure 3.3(b), for $\gamma = 90^o$ and 180^o, the isotherms travel through out the cavity where as for the case of pure fluid, isotherms are mostly restricted to the left side of the cavity accept for the case of $\gamma = 90^o$ and 180^o in which isotherms travel up to the middle of cavity.

Now for mixed convection case $Ri = 1$ with $Re = 100$, Figure 3.4 and Figure 3.5 shows typical contour mapping for streamlines and isotherms. As Figure 3.4(a) illustrate the flow regime in the channel cavity with functions of inclination angle. For $Ri = 1$, a large recirculating cell is seen in the cavity showing the movement of fluid flow by the contours with no change in the angle position. When inclination angle is increased, the cell starts declining. The longitudinal eddy completely vanishes up to $\gamma = 180^o$ because shear and buoyancy forces plays equal role in the flow movement. In Figure 3.4(b), the thickness of layer increases with the increased inclination angle. For $\gamma = 180^o$, thermal boundary layer is strongly induced near the left hot wall of the cavity showing the dominant thermal conduction. As the intensity of heat is seen to be decreased when the flow moves away from it. Figure 3.5(a)

and Figure 3.5(b) shows the depiction of flow directions in nanofluid. Greater intensity of nanoparticles ϕ shown in Figure 3.5 demonstrates the increased Nu_{avg} as compared to base fluid case. Flow strength near the upper wall of the channel induces strong effect as the flow velocity weakens near the cavity. The overall heat transfer rate is increased for streamlines and isotherms in the case of nanofluid.

Observing the effect of different Reynolds number $100 \leq Re \leq 400$, Figure 3.6 and Figure 3.7 illustrate streamlines and isotherms for $Ri = 0.04$. Figure 3.6(a) shows the velocity of pure fluid in the channel with cavity. As we can see clearly, a longitudinal zone is seen in the cavity at $Re = 100$ but increment in the Re lessens the effect of eddy by the flow movement. So the increase in the Re, weakens the flow strength in the cavity. Similarly demonstrating the temperature gradient in Figure 3.6(b), the behaviour flow regime effects the thermal conduction. Dominant shear forces strongly effects the thermal boundary layer. Increasing Re, gradually decreases the thermal layer which shows the strong effect of shear forces on the fluid flow in the cavity. Figure 3.7 depicts the movement of flow with the inducement of nanoparticles. Similar effect is shown in both cases with the slight increase in heat transfer. As strength of flow is decreased to minimum level in the centers of recirculating zone. Figure 3.7(b) shows the increase change of temperature in the flow at $Re = 200$ by contour mapping as compared to Figure 3.6(b).

Similar variation of Reynolds number is also observed for $Ri = 1$ with $\gamma = 0^o$. Figure 3.8(a) shows a large cell covering the whole cavity at $Re = 100$. When Re is increased to 200, the contours near left bottom end start weakening. At $Re = 400$, small cell shows the lesser effect of velocity in the cavity. Figure 3.8(b) represents the thermal layer due to isotherms. Increase contribution of Reynolds number Re, gradually lightens the thickness of boundary layer. The thickness of thermal layer is weaker as compared to $Ri = 0.04$ because shear and buoyancy forces are equally dominant. Figure 3.9(a) and Figure 3.9(b) illustrate the streamlines and isotherms with nanofluid. As average Nusselt number is increased with the induction of solid volume fraction. Figure 3.10 represents the strong effect of ϕ in various cases for $\phi = 0$, 0.02, 0.04 and 0.06. The influence of solid volume fraction is discussed in mixed convection regime. We can see clearly in Figure 3.10, the effect of solid volume fraction on inclined channel with cavity is dominant. The maximum heat transfer rate increases with the increase in ϕ's in mixed convection. Figure 3.11 and Figure 3.12 depicts the variation of Re in forced regime and mixed regime. Both cases demonstrates the same conclusion i.e., increasing the Reynolds number Re, average Nusselt number Nu_{avg} also increases in inclined channel with cavity.

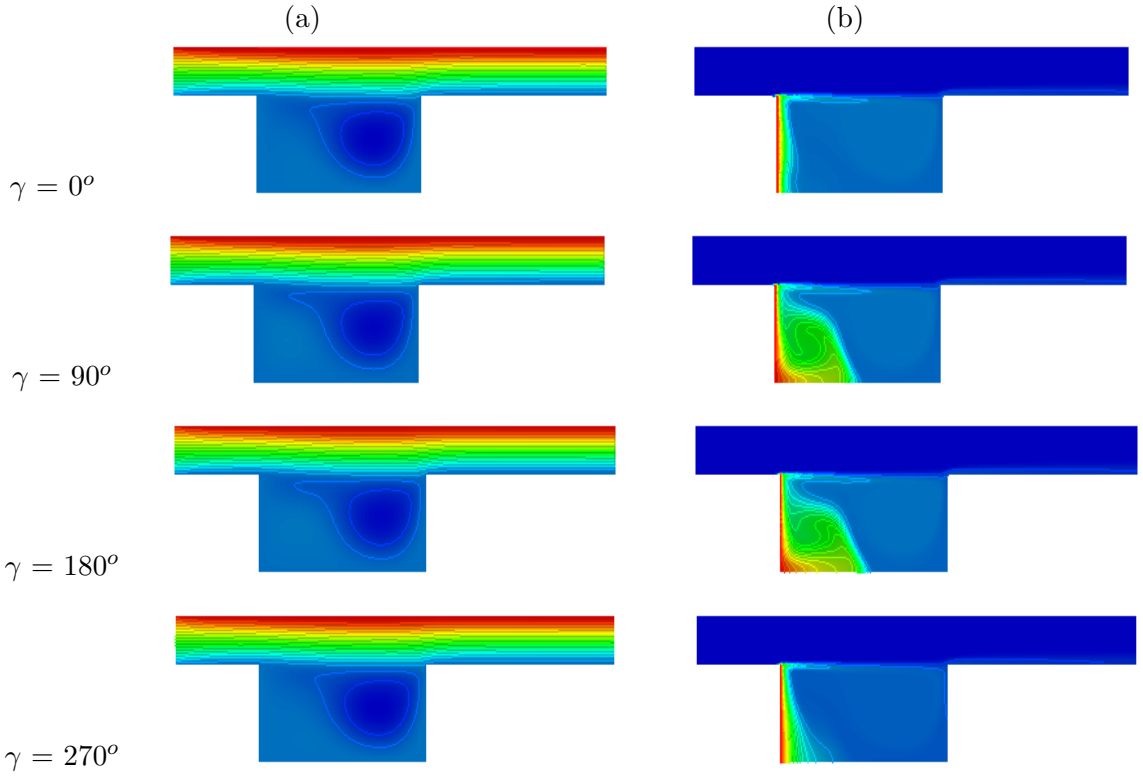

FIGURE 3.2: Influence of different inclination angle γ on (a) streamlines (b) isotherms with $Ri = 0.04$, $Re = 500$ at $\phi = 0$.

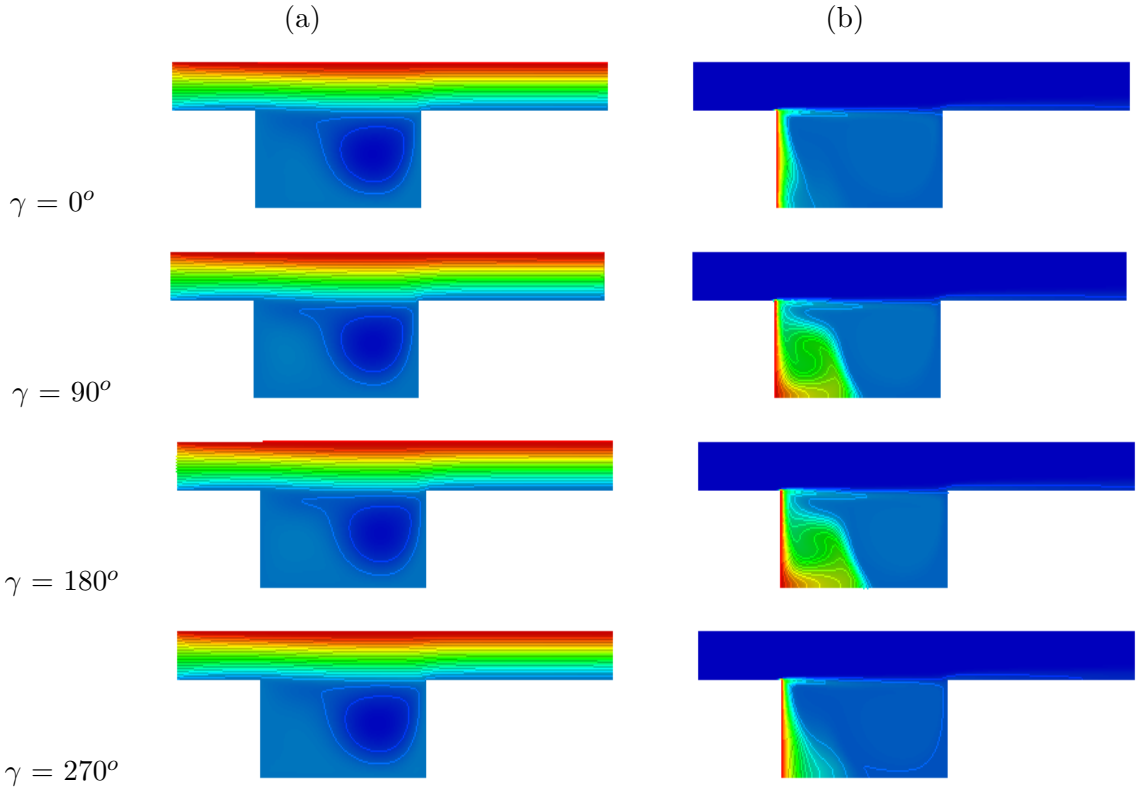

FIGURE 3.3: Influence of different inclination angle γ on (a) streamlines (b) isotherms with $Ri = 0.04$, $Re = 500$ at $\phi = 0.06$.

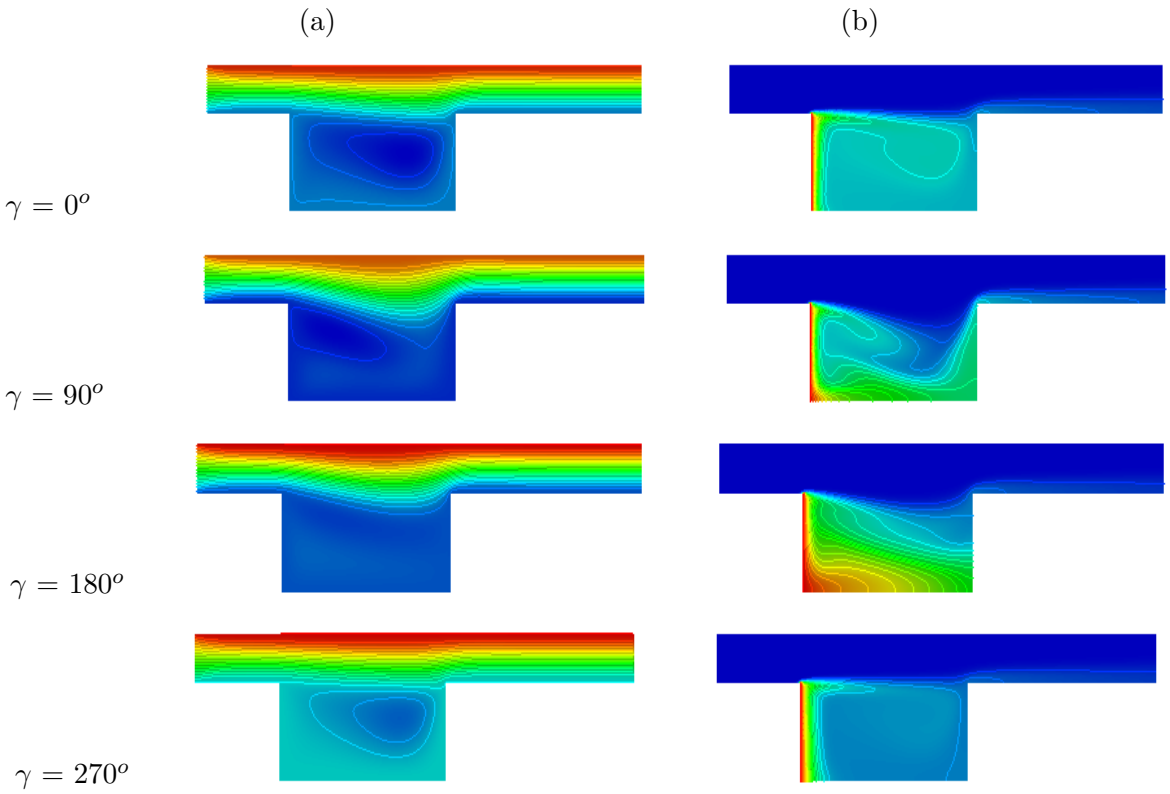

FIGURE 3.4: Influence of different inclination angle γ on (a) streamlines and (b) isotherms with $Ri = 1$, $Re = 100$ at $\phi = 0$.

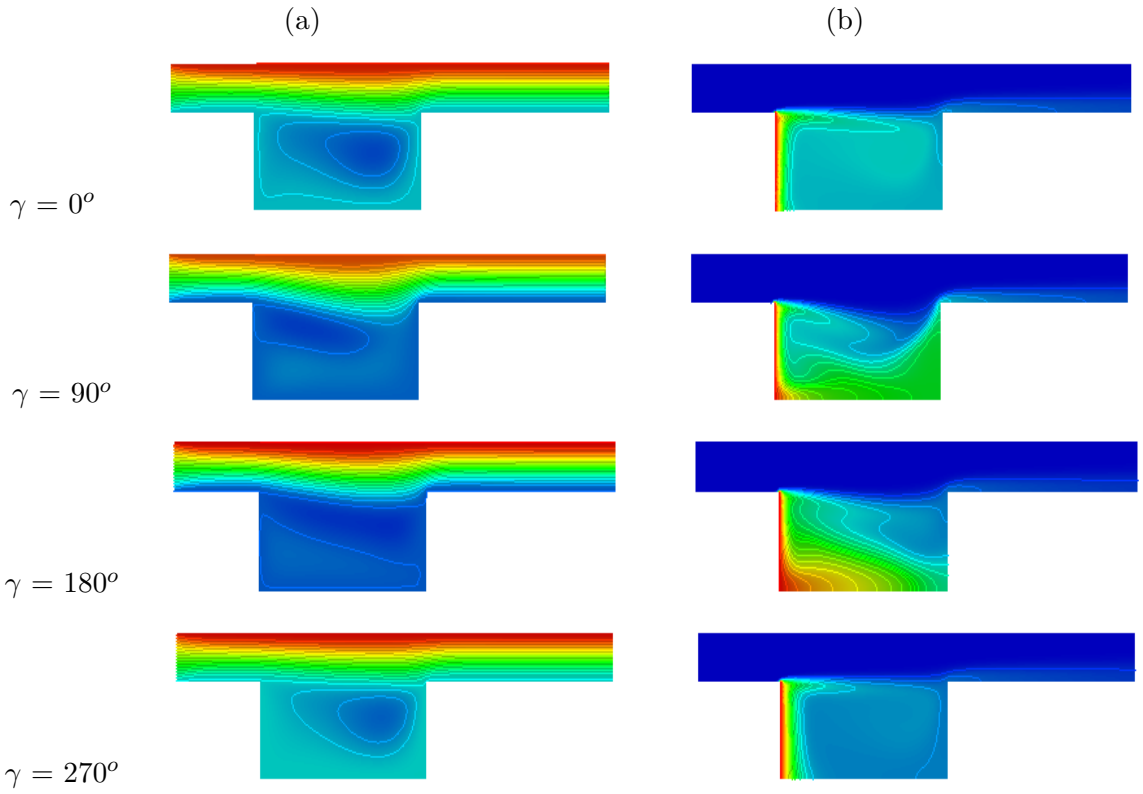

FIGURE 3.5: Influence of different inclination angle γ on (a) streamlines and (b) isotherms with $Ri = 1$, $Re = 100$ at $\phi = 0.06$.

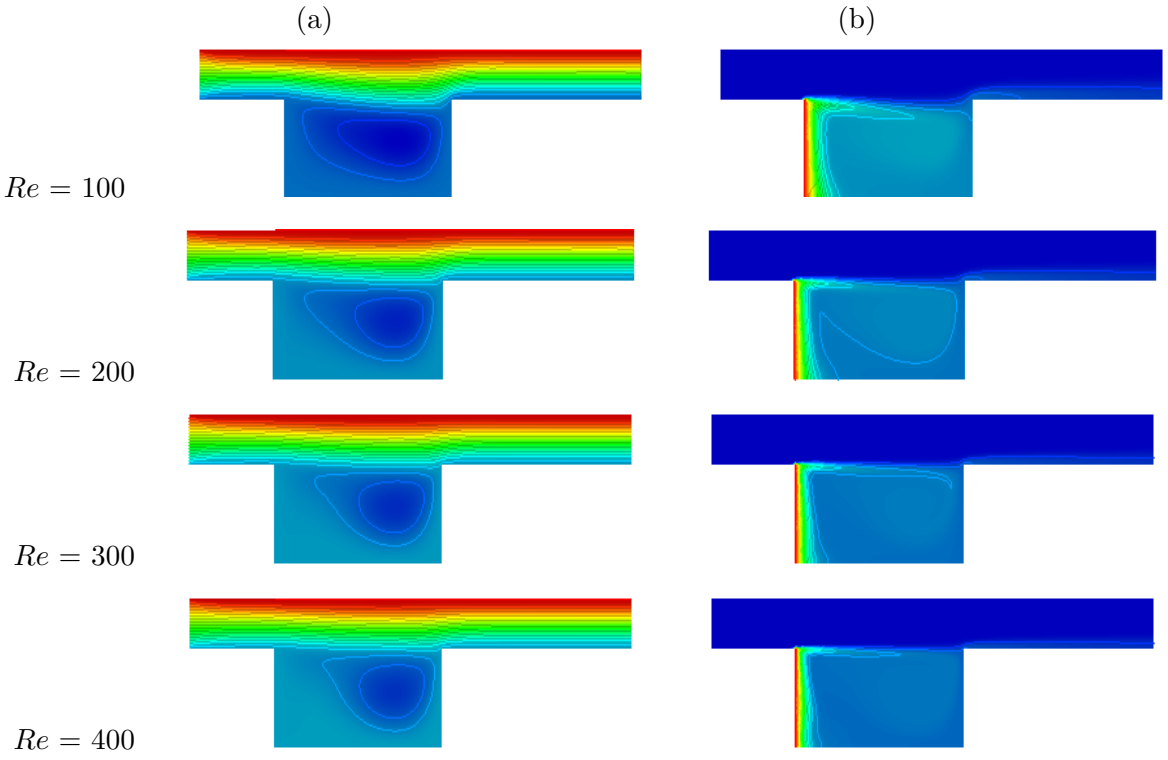

FIGURE 3.6: Influence of different Reynolds number at $100 \leq Re \leq 400$ on (a) streamlines (b) isotherms with $Ri = 0.04$ and $\phi = 0$.

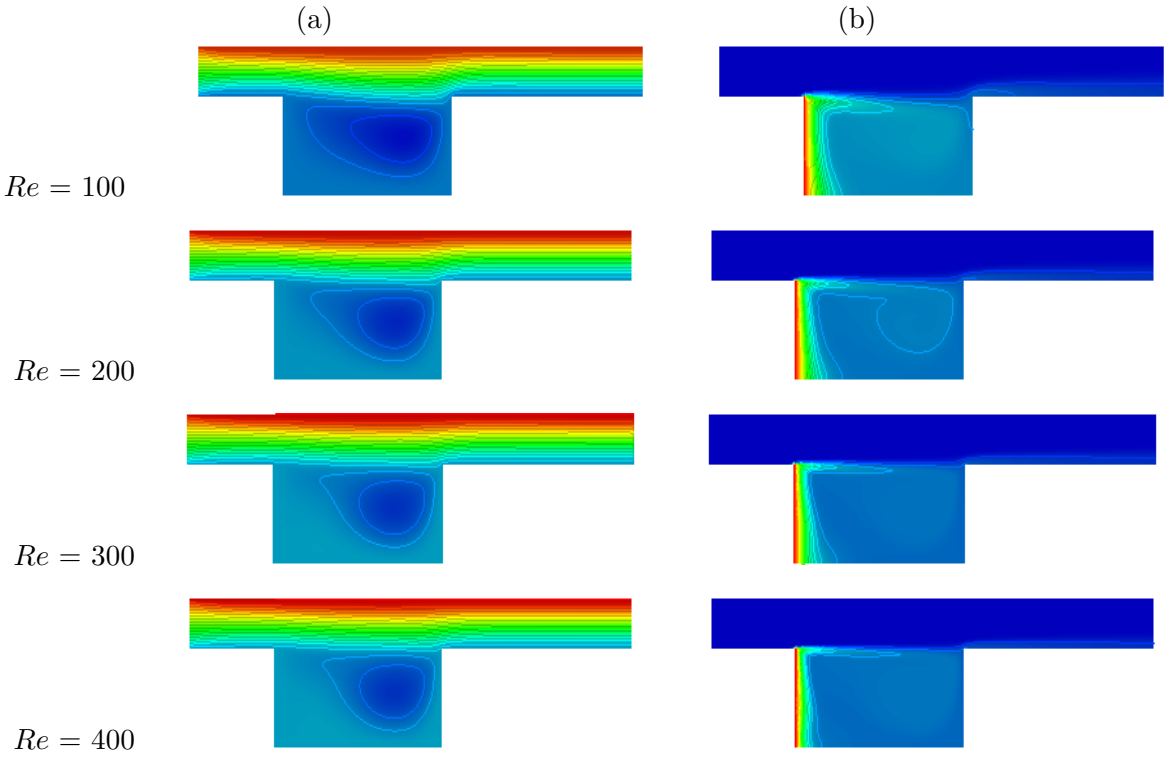

FIGURE 3.7: Influence of different Reynolds number at $100 \leq Re \leq 400$ on (a) streamlines (b) isotherms with $Ri = 0.04$, $\phi = 0.06$.

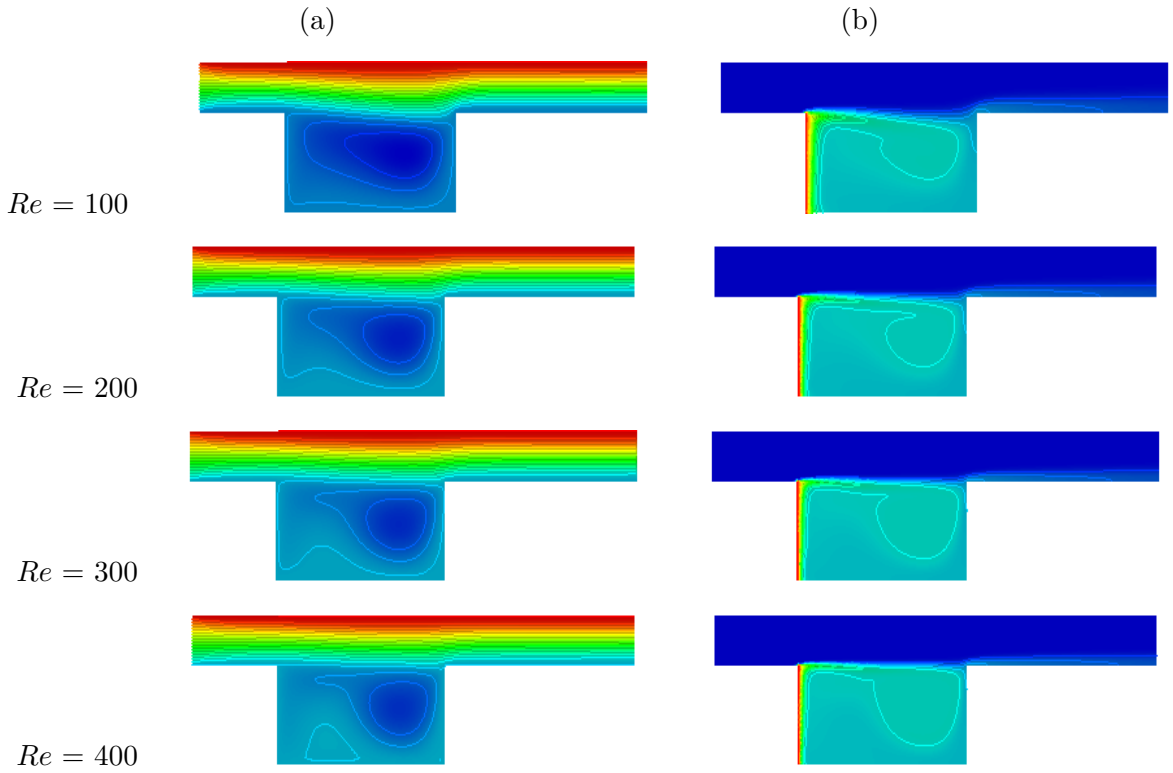

FIGURE 3.8: Influence of different Reynolds number at $100 \leq Re \leq 400$ on (a) streamlines (b) isotherms with $Ri = 1$, $\phi = 0$.

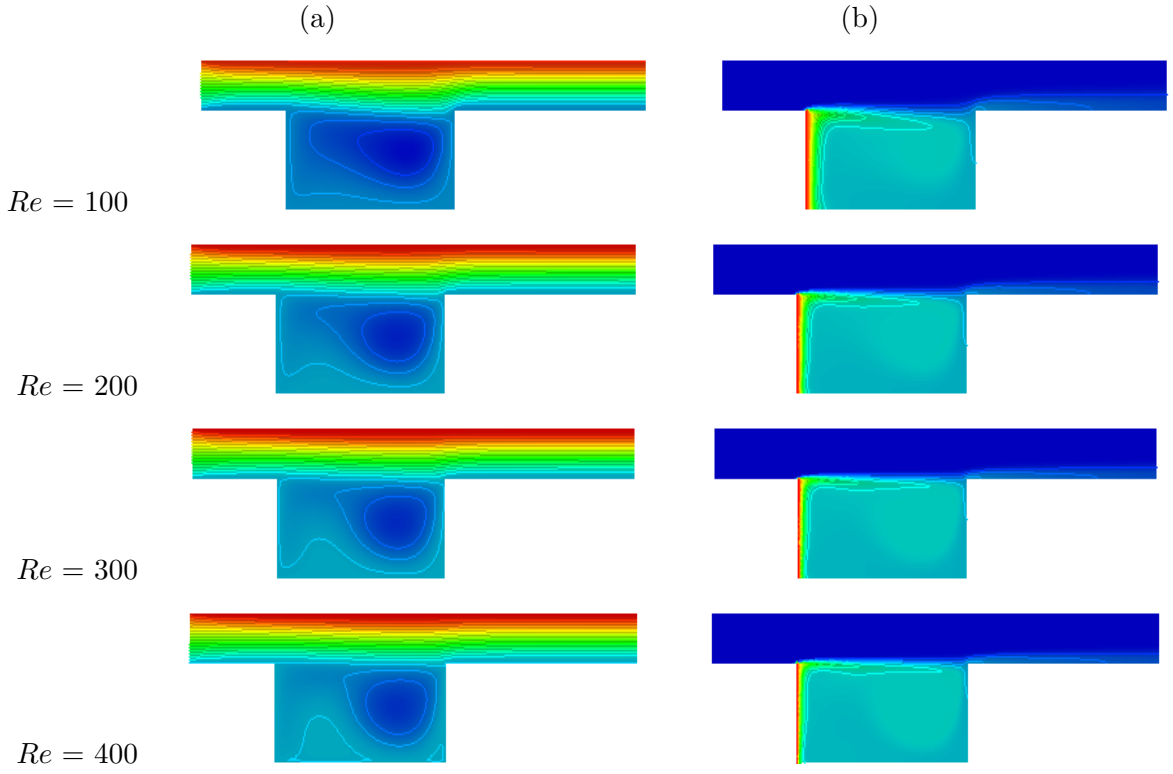

FIGURE 3.9: Influence of different Reynolds number at $100 \leq Re \leq 400$ on (a) streamlines (b) isotherms with $Ri = 1$, $\phi = 0.06$.

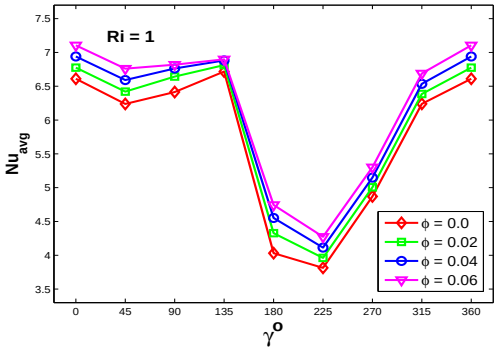

(a)

FIGURE 3.10: Influence of solid volume fraction on the average Nusselt number as a function of inclination angle with $Ri = 1$ and $Re = 100$.

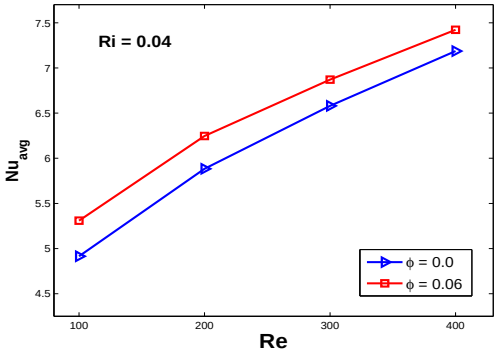

(a)

FIGURE 3.11: Influence of forced convection on average Nusselt number as function of $100 \leq Re \leq 400$ with $\gamma = 0^o$.

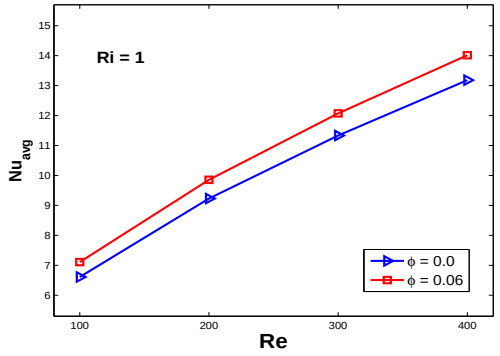

(a)

FIGURE 3.12: Influence of mixed convection on average Nusselt number as function of $100 \leq Re \leq 400$ with $\gamma = 0^o$.

Chapter 4

Numerical simulation of mixed convective nanofluid in inclined channel cavity in porous medium

The main objective of this present phenomenon is to consider the Brinkmam Darcy model implemented on the momentum equation for both x, y components of mixed convection in horizontal open cavity with inclination angle inducing in porous medium through the channel. Copper nanoparticles are saturately involved with water to show the intensity of fluid where as Darcy number Da, Grashof number Gr are also varied for three different convection regimes briefly explained below.

4.1 Geometry of the Flow and Mathematical Analysis of Governing Equations

The present work considers two dimensional and laminar flow of incompressible, newtonian fluid in an inclined open channel with cavity in porous medium with cavity height H and channel height w. Boussinesq approximation is applied with the constant fluid properties of copper particles as shown in the Table 3.1. The porous medium is considered to be saturated with fluid. Assuming the pure fluid (water) and Cu - spherical particles which are in thermal equilibrium. Left side of the wall has uniform heat distribution T_H and flow enters through the left side of the channel at constant temperature T_C. The remaining walls of cavity are adiabatic. The size and shape of solid particles are characterized as uniform. Demonstrative effect is shown on fluid flow by considering different Reynolds numbers. The analysis of flow of fluid in the cavity is being optimized by streamlines, isotherms and average Nusselt

numbers. Taking in account the above assumptions and in consideration of Boussinesq approximation two dimensional equations consisting of mass, momentum and energy [13] for mixed convection flow in porous cavity of nanofluid are shown below

Continuity equation

$$\frac{\partial u}{\partial x}+\frac{\partial v}{\partial y}=0, \tag{4.1}$$

x - Momentum equation

$$\rho_{nf}\left(u\frac{\partial u}{\partial x}+v\frac{\partial u}{\partial y}\right)=-\frac{\partial p}{\partial x}+\mu_{nf}\left(\frac{\partial^2 u}{\partial x^2}+\frac{\partial^2 u}{\partial y^2}\right)+(\rho\beta)_{nf}g(T-T_c)(\sin\gamma)-\frac{\mu_f}{\rho_f}\frac{u}{\kappa}, \tag{4.2}$$

y - Momentum equation

$$\rho_{nf}\left(u\frac{\partial v}{\partial x}+v\frac{\partial v}{\partial y}\right)=-\frac{\partial p}{\partial y}+\mu_{nf}\left(\frac{\partial^2 v}{\partial x^2}+\frac{\partial^2 v}{\partial y^2}\right)+(\rho\beta)_{nf}g(T-T_c)(\cos\gamma)-\frac{\mu_f}{\rho_f}\frac{v}{\kappa}, \tag{4.3}$$

Energy equation

$$u\frac{\partial T}{\partial x}+v\frac{\partial T}{\partial y}=\frac{\alpha_{nf}}{\alpha_f}\frac{1}{RePr}\left(\frac{\partial^2 T}{\partial x^2}+\frac{\partial^2 T}{\partial y^2}\right). \tag{4.4}$$

Here u, v expresses the component of velocity along x-direction and y-direction respectively, p denotes the fluid pressure, β is the volumetric thermal expansion coefficient, κ shows the permeability of the porous medium, T is the temperature and γ expresses the inclination angle of the channel cavity in the horizontal direction. ϕ expresses base fluid with the contribution of nanoparticles of copper. The dimensional forms of boundary conditions are given below

- On the inlet side of the channel:

$$u=1, \quad v=0, \quad T=0 \ \ (T=T_C) \tag{4.5}$$

- On the left wall of the cavity:

$$u=0, \quad v=0, \quad T=1 \ \ (T=T_H) \tag{4.6}$$

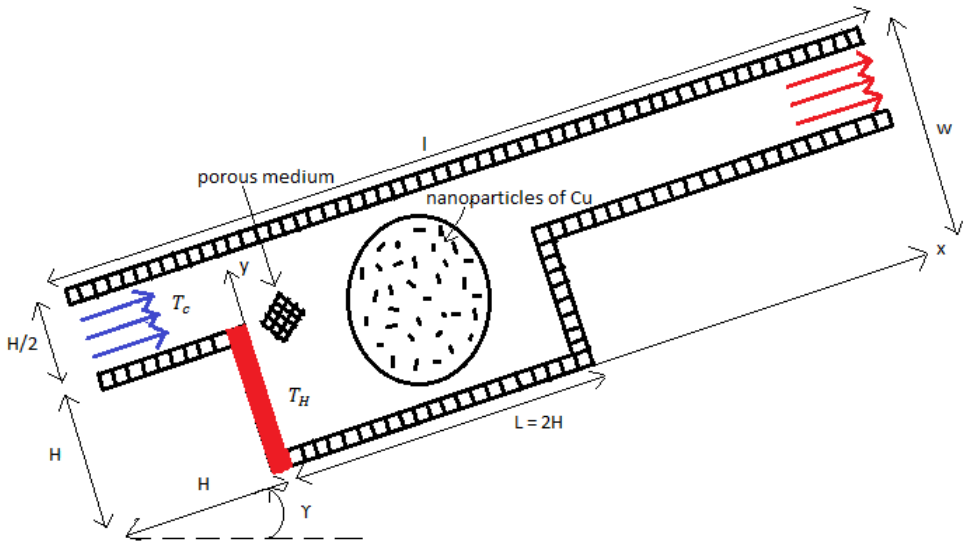

FIGURE 4.1: Physical model of schematic diagram.

- On the rest adiabetic walls of the channel and cavity:

$$u = 0, \quad v = 0, \quad \frac{\partial T}{\partial y} = 0 \ \text{(for horizontal wall)} \quad \text{and} \quad \frac{\partial T}{\partial x} = 0 \ \text{(for vertical wall)}. \tag{4.7}$$

- On the outlet side of the channel:

$$\frac{\partial u}{\partial x} = 0, \quad \frac{\partial v}{\partial y} = 0, \quad \frac{\partial T}{\partial x} = 0. \tag{4.8}$$

4.2 Non-dimensional Form of the Governing Equations:

Reducing the above governing equations from Eqs. (4.1) - (4.4), into dimensionless form, the following parameters are involved

$$Re = \frac{\rho_f u_o H}{\mu_f} \quad (The\ Reynolds\ number),$$

$$Da = \frac{\kappa}{H^2} \quad (The\ Darcy\ number),$$

As non-dimensional variables are defined as:

$X = \frac{x}{H}$, $Y = \frac{y}{H}$, $U = \frac{u}{u_o}$, $V = \frac{v}{u_o}$, $P = \frac{p}{\rho_{nf} u_o^2}$, $\theta = \frac{(T - T_C)}{(T_H - T_C)}$.

By using these dimensionless parameters and variables, the above governing equations are

categorized in this way given below:

$$\frac{\partial U}{\partial X}+\frac{\partial V}{\partial Y}=0, \tag{4.9}$$

$$U\frac{\partial U}{\partial X}+V\frac{\partial U}{\partial Y}=-\frac{\partial P}{\partial X}+\frac{1}{Re}\frac{\rho_f}{\rho_{nf}}\frac{1}{(1-\phi)^{2.5}}\left(\frac{\partial^2 U}{\partial X^2}+\frac{\partial^2 U}{\partial Y^2}\right) + Ri\frac{\rho_f}{\rho_{nf}}\left((1-\phi+\frac{\rho_s\beta_s\phi}{\rho_f\beta_f}\right)(\sin\gamma)\theta-\frac{1}{ReDa}\frac{U}{\rho_{nf}}, \tag{4.10}$$

$$U\frac{\partial V}{\partial X}+V\frac{\partial V}{\partial Y}=-\frac{\partial P}{\partial Y}+\frac{1}{Re}\frac{\rho_f}{\rho_{nf}}\frac{1}{(1-\phi)^{2.5}}\left(\frac{\partial^2 V}{\partial X^2}+\frac{\partial^2 V}{\partial Y^2}\right) + Ri\frac{\rho_f}{\rho_{nf}}\left((1-\phi+\frac{\rho_s\beta_s\phi}{\rho_f\beta_f}\right)(\cos\gamma)\theta-\frac{1}{ReDa}\frac{V}{\rho_{nf}}, \tag{4.11}$$

$$U\frac{\partial \theta}{\partial X}+V\frac{\partial \theta}{\partial Y}=\frac{\alpha_{nf}}{\alpha_f}\frac{1}{RePr}\left(\frac{\partial^2 \theta}{\partial X^2}+\frac{\partial^2 \theta}{\partial Y^2}\right). \tag{4.12}$$

The appropiate dimensionless boundary conditions of governing problem are as given below:

- On the inlet side of the channel:

$$U=1, \quad V=0, \quad \theta=0 \tag{4.13}$$

- On the left wall of the cavity:

$$U=0, \quad V=0, \quad \theta=1 \tag{4.14}$$

- On the rest adiabatic walls of the channel and cavity:

$$U=0, \quad V=0, \quad \frac{\partial \theta}{\partial Y}=0 \ \text{(for horizontal wall)} \quad \text{and} \quad \frac{\partial \theta}{\partial X}=0 \ \text{(for vertical wall).} \tag{4.15}$$

- On the outlet side of the channel:

$$\frac{\partial U}{\partial X}=0 \quad \frac{\partial V}{\partial Y}=0 \quad \frac{\partial \theta}{\partial X}=0. \tag{4.16}$$

The nanofluid properties are shown in Table 3.2.

4.3 Numerical Procedure

The system of coupled non-linear partial differential equations Eqs. (4.9) - (4.12) together with the boundary conditions (4.13) - (4.16) have been discretized numerically by finite element method with adapted grid together with Galerkin weighted residual technique. Using the finite element method, equations are converted into system of algebraic equations through integration dependent on whole domain where U, V and θ are discretized by Q_2 element of 3rd order accuracy and P is discretized by $P_1{}^{\text{disc}}$ element of 2nd order accuracy(see [30] for details). It is transformed into 4 x 4 matrix with the adaptation of laplace, mass and convective matrix including non-linearity terms. The average Nusselt number is the analyzed for overall heat transfer rate. It considers the effect of invoking different inclination angles in the channel with working nanofluid of Cu-water on mixed convection saturated with porous medium. We have obtained the results by streamlines and isotherms.

4.3.1 Variational Formulation of Governing Equations

In this section, Eqs. (4.9) - (4.12) illustrate from strong form to weaker form. Multiplier method / Weak form or the Variational formulation method is an approach where the governing equations are multiplied by suitable functions known as test functions w, q and then integrated over the whole domain Ω.

$$\frac{\partial U}{\partial X}+\frac{\partial V}{\partial Y}=0, \tag{4.17}$$

$$U\frac{\partial U}{\partial X}+V\frac{\partial U}{\partial Y}=-\frac{\partial P}{\partial X}+\frac{1}{Re}\frac{\rho_f}{\rho_{nf}}\frac{1}{(1-\phi)^{2.5}}\left(\frac{\partial^2 U}{\partial X^2}+\frac{\partial^2 U}{\partial Y^2}\right) + Ri\frac{\rho_f}{\rho_{nf}}\left(1-\phi+\frac{\rho_s\beta_s\phi}{\rho_f\beta_f}\right)(\sin\gamma)\theta-\frac{1}{ReDa}\frac{U}{\rho_{nf}}, \tag{4.18}$$

$$U\frac{\partial V}{\partial X}+V\frac{\partial V}{\partial Y}=-\frac{\partial P}{\partial Y}+\frac{1}{Re}\frac{\rho_f}{\rho_{nf}}\frac{1}{(1-\phi)^{2.5}}\left(\frac{\partial^2 V}{\partial X^2}+\frac{\partial^2 V}{\partial Y^2}\right) + Ri\frac{\rho_f}{\rho_{nf}}\left(1-\phi+\frac{\rho_s\beta_s\phi}{\rho_f\beta_f}\right)(\cos\gamma)\theta-\frac{1}{ReDa}\frac{V}{\rho_{nf}}, \tag{4.19}$$

$$U\frac{\partial \theta}{\partial X}+V\frac{\partial \theta}{\partial Y}=\frac{\alpha_{nf}}{\alpha_f}\frac{1}{RePr}\left(\frac{\partial^2 \theta}{\partial X^2}+\frac{\partial^2 \theta}{\partial Y^2}\right). \tag{4.20}$$

Let W = $[H^1(\Omega)]^3$ shows the test spaces for u-velocity, v-velocity and temperature where Q = $L^2(\Omega)$ shows the test space for pressure. The variational form of governing equations is given as

Find $(U,\, V,\, \theta,\, P)\ \epsilon\ \mathrm{W} \times \mathrm{Q}$ such that

$$-\frac{\rho_f}{\rho_{nf}}\frac{1}{(1-\phi)^{2.5}}\int_\Omega \frac{1}{Re}\left(\frac{\partial^2 U}{\partial X^2}+\frac{\partial^2 U}{\partial Y^2}\right)\ w\ d\Omega+\int_\Omega\left(U\frac{\partial U}{\partial X}+V\frac{\partial U}{\partial Y}\right)\ w\ d\Omega+\int_\Omega\frac{\partial P}{\partial X}\ w\ d\Omega$$
$$-Ri\frac{\rho_f}{\rho_{nf}}\left(1-\phi+\frac{\rho_s\beta_s\phi}{\rho_f\beta_f}\right)(\sin\gamma)\int_\Omega\theta\ w\ d\Omega+\frac{1}{ReDa}\frac{1}{\rho_n f}\int_\Omega U\ w\ d\Omega=0, \tag{4.21}$$

$$-\frac{\rho_f}{\rho_{nf}}\frac{1}{(1-\phi)^{2.5}}\int_\Omega \frac{1}{Re}\left(\frac{\partial^2 V}{\partial X^2}+\frac{\partial^2 V}{\partial Y^2}\right)\ w\ d\Omega+\int_\Omega\left(U\frac{\partial V}{\partial X}+V\frac{\partial V}{\partial Y}\right)\ w\ d\Omega+\int_\Omega\frac{\partial P}{\partial Y}\ w\ d\Omega$$
$$-Ri\frac{\rho_f}{\rho_{nf}}\left(1-\phi+\frac{\rho_s\beta_s\phi}{\rho_f\beta_f}\right)(\cos\gamma)\int_\Omega\theta\ w\ d\Omega+\frac{1}{ReDa}\frac{1}{\rho_n f}\int_\Omega V\ w\ d\Omega=0, \tag{4.22}$$

$$\int_\Omega\left(\frac{\partial U}{\partial X}+\frac{\partial V}{\partial Y}\right)\ q\ d\Omega=0, \tag{4.23}$$

$$\int_\Omega\left(U\frac{\partial\theta}{\partial X}+V\frac{\partial\theta}{\partial Y}\right)\ w\ d\Omega-\frac{\alpha_{nf}}{\alpha_f}\frac{1}{RePr}\int_\Omega\left(\frac{\partial^2\theta}{\partial X^2}+\frac{\partial^2\theta}{\partial Y^2}\right)\ w\ d\Omega=0. \tag{4.24}$$

for all $(w,\, q)\ \epsilon\ \mathrm{W} \times \mathrm{Q}$.

By Galerkin approximation

$$\frac{\rho_f}{\rho_{nf}}\frac{1}{(1-\phi)^{2.5}}\int_\Omega\frac{1}{Re}\left(\frac{\partial U_h}{\partial X}\ \frac{\partial w_h}{\partial X}+\frac{\partial U_h}{\partial Y}\ \frac{\partial w_h}{\partial Y}\right)\ d\Omega+\int_\Omega\left(U_h\frac{\partial U_h}{\partial X}+V_h\frac{\partial U_h}{\partial Y}\right)\ w_h\ d\Omega-$$
$$Ri\frac{\rho_f}{\rho_{nf}}\left(1-\phi+\frac{\rho_s\beta_s\phi}{\rho_f\beta_f}\right)(\sin\gamma)\int_\Omega\theta_h\ w_h\ d\Omega+\frac{1}{ReDa}\frac{1}{\rho_n f}\int_\Omega U_h\ w_h\ d\Omega\int_\Omega\frac{\partial P_h}{\partial X}\ w_h\ d\Omega=0, \tag{4.25}$$

$$\frac{\rho_f}{\rho_{nf}}\frac{1}{(1-\phi)^{2.5}}\int_\Omega\frac{1}{Re}\left(\frac{\partial V_h}{\partial X}\ \frac{\partial w_h}{\partial X}+\frac{\partial V_h}{\partial Y}\ \frac{\partial w_h}{\partial Y}\right)\ d\Omega+\int_\Omega\left(U_h\frac{\partial V_h}{\partial X}+V_h\frac{\partial V_h}{\partial Y}\right)\ w_h\ d\Omega-$$
$$Ri\frac{\rho_f}{\rho_{nf}}\left(1-\phi+\frac{\rho_s\beta_s\phi}{\rho_f\beta_f}\right)(\cos\gamma)\int_\Omega\theta_h\ w_h\ d\Omega+\frac{1}{ReDa}\frac{1}{\rho_n f}\int_\Omega V_h\ w_h\ d\Omega\int_\Omega\frac{\partial P_h}{\partial Y}\ w_h\ d\Omega=0, \tag{4.26}$$

$$\int_\Omega\left(\frac{\partial U_h}{\partial X}+\frac{\partial V_h}{\partial Y}\right)\ q_h\ d\Omega=0, \tag{4.27}$$

$$\int_\Omega\left(U_h\frac{\partial\theta_h}{\partial X}+V_h\frac{\partial\theta_h}{\partial Y}\right)\ w_h\ d\Omega+\frac{\alpha_{nf}}{\alpha_f}\frac{1}{RePr}\int_\Omega\left(\frac{\partial\theta_h}{\partial X}\ \frac{\partial w_h}{\partial X}+\frac{\partial\theta_h}{\partial Y}\ \frac{\partial w_h}{\partial Y}\right)\ d\Omega=0. \tag{4.28}$$

.

Using FEM approximation of U_h, V_h, θ_h and P_h. In the same way converting $(w,\, q)$ test functions into basis functions as w_h, q_h.

The fully discretized system reads the following :

$$\underbrace{\begin{pmatrix} a_{11}L + b_{11}M + N(\underline{U},\underline{V}) & 0 & B_1 & b_{14}M \\ 0 & a_{22}L + b_{22}M + N(\underline{U},\underline{V}) & B_2 & b_{24}M \\ B_1^T & B_2^T & 0 & 0 \\ 0 & 0 & 0 & a_{44}L + N(\underline{U},\underline{V}) \end{pmatrix}}_{\text{A}} \underbrace{\begin{pmatrix} \underline{U} \\ \underline{V} \\ \underline{P} \\ \underline{\theta} \end{pmatrix}}_{\text{U}} = \underbrace{\begin{pmatrix} 0 \\ 0 \\ 0 \\ 0 \end{pmatrix}}_{\text{B}}, \tag{4.29}$$

where A is known as "block matrix", U is called "solution vector" and B is expressed as "load vector" In block matrix,

$$\begin{aligned} a_{11} &= \frac{1}{Re}\frac{\rho_f}{\rho_{nf}}\frac{1}{(1-\phi)^{2.5}} = a_{22}, \\ a_{44} &= \frac{\alpha_{nf}}{\alpha_f}\frac{1}{RePr}, \\ b_{11} &= \frac{1}{ReDa}\frac{1}{\rho_{nf}} = b_{22}, \\ b_{14} &= -Ri\frac{\rho_f}{\rho_{nf}}\left(1-\phi+\frac{\rho_s\beta_s\phi}{\rho_f\beta_f}\right)(\sin\gamma), \\ b_{24} &= -Ri\frac{\rho_f}{\rho_{nf}}\left(1-\phi+\frac{\rho_s\beta_s\phi}{\rho_f\beta_f}\right)(\cos\gamma). \end{aligned}$$

where L, M and N are the Laplace, mass and convective matrix. Similarly, B_1 and B_2 are the pressure matrix with their tranpose B_1^T and B_2^T.

4.4 Results and Discussion

The present investigation involves the governing parameters such as the Richardson number showing the influence of buoyancy forces, the Darcy number identifying the relative effect of porous medium and permeability. The strength of motion inside cavity is characterized by Reynolds number Re and also the Grashof number Gr for making the buoyancy forces more prominant on the flow inside the channel with cavity. The values of Reynolds number are taken as 10 and 50 whereas Gr is considered to be 10^2 and 10^4 in the following discussion. Furthermore, three different regimes are discussed to show the significance of fluid flow inside cavity, i.e., $Ri > 1$ for natural convection, $Ri < 1$ for forced convection and $Ri = 1$ for mixed convection. Darcy number is changed from 10^{-4} to ∞, i.e., $Da = \infty$ shows the non-existence of porous medium by fixing the prandtl number $Pr = 6.2$. Nanoparticles are assumed to be

$\phi = 0$, 0.02. 0.04 and 0.06 and the inclination angle of channel is supposed to be $\gamma = 0^o$, 90^o, 180^o and 270^o.

Figure 4.2 depicts the streamlines and isotherms for $Ri = 1$ with porous medium $Da = 10^{-4}$. For different inclination angles, strength of fluid motion is seen in Figure 4.2(a) for pure fluid. Strong resolution of flow is observed near the upper wall of the channel where flow is invoked through inlet. Furthermore, a parabolic bell shaped contour is noticed in the cavity. At $\gamma = 180^o$, the horizontal curve is fully centered which shows that shear forces and buoyancy forces are acting equally. In Figure 4.2(b), isotherms represents the temperature contours near the hot wall. Thermal conduction produces by the involvement of porosity. Temperature near the heated wall shows an increase in the thickness of thermal boundary layer. Thermal boundary layer seems to be thicker at $\gamma = 180^o$ and seems to be thin for $\gamma = 270^o$. Similar in the case for nanofluid shown in Figure 4.3 in which intensity in the fluid increases with the effect of solid volume fraction ϕ.

Figure 4.4 shows the influence of natural convection in the pure fluid. A double layered vortex is shown in Figure 4.4(a) shows strong strength near the upper wall of the channel. Induced circulating cell shows the weak flow motion in the cavity for $\gamma = 0^o$. For $\gamma = 90^o$, strong flow paths covers the channel moving towards the cavity. Similarly, presentation of isotherms show the temperature enhancement near the heated wall in Figure 4.4(b). Thin boundary layer is produced for $\gamma = 0^o$, as moving towards $\gamma = 90^o$, thickness of thermal boundary layer seems to be greater. For the case of nanofluid, intensity in the fluid increases due to which Figure 4.5(a) shows a slight change within the cavity in the circulating zone. In Figure 4.5(b), increment of temperature is seen near the left heated wall. Heat transfer is increased for the presence of nanoparticles which can be observed along the walls of the cavity in Figure 4.5(b).

Figure 4.6 illustrate the strong effect of ϕ in various cases with for $\phi = 0$, 0.02, 0.04 and 0.06. All the effects of solid volume fraction are discussed in three different convection regimes such as $Ri < 1$, $Ri > 1$ and $Ri = 1$. In this figure, Darcy number is taken as $Da = 10^{-2}$ which shows the high porous medium obtaining maximum heat transfer rate in the horizontal channel with cavity. Figure 4.6(a) considers $Ri = 0.01$ where the average Nusselt number for the dominating forced convection shows the slight curvy down at $\gamma = 180^o$. Moreover, maximum Nu_{avg} is acquired for $\gamma = 0^o$ and 360^o. Figure 4.6(b) considers $Ri = 1$ where the average Nu_{avg} shows the maximum heat transfer rate at $\gamma = 135^o$. Similar case for $Ri = 100$ in Figure 4.6(c), average Nusselt number increases at $\gamma = 90^o$. Since the effect of solid volume fraction ϕ in the inclined open porous cavity is prominent, i.e., the overall average Nusselt number Nu_{avg} increases with the increase of ϕ for all Ri considering in the porous medium. Furthermore, average Nu_{avg} decreases with the increment of all considered

Ri. Figure 4.7 shows the influence of forced convection when $Ri = 0.01$, $Gr = 10^2$, $\gamma = 0^o$ considering fluids, base fluid in Figure 4.7(a) and nanofluid in Figure 4.7(b). The main purpose of changing the Darcy number is to illustrate the heat transfer rate in forced convection regime. In Figure 4.7(a), we can see the effect of Darcy number for ∞, 10^{-4}, 10^{-3}, 10^{-2} and 10^{-1} on heat transfer rate as shown graphically. For non porous medium where porosity is completely neglected, shows the decreased average Nusselt number.

Furthermore, with an increase in Da, heat transfer exchange increases. As increasing the darcy number results in the increment of thermal conductivity of the fluid. Thus, noted that thermal boundary layer induced by the temperature gradient near left wall of cavity thickens due to increasing Darcy number. Same is the case for nanofluid, as induction of porous medium increases the intensity in the fluid flow. Graphs presented for mixed convection ($Ri = 1$) shows for both fluids in Figure 4.8. Similar results are illustrated for this convection regime by changing the Darcy number Da at various points and also shown for non porous medium. Nu_{avg} increases slightly by increasing the Darcy number present in Brinkman Darcy equation(BDE). For nanofluid case obtaining the same result as heat transfer rate is increased with the addition of nanoparticles and for Natural convection regime ($Ri = 100$) in Figure 4.9, similar results are shown. Figure 4.10 shows the influence of Grashof number Gr on the inclined non-porous cavity. Natural and forced convection in nonporous medium $Da = \infty$ for $Gr = 10^2$ and $Gr = 10^4$ are considered. Figure 4.10(a) shows the highest average Nusselt number for $Ri = 0.01$, $Gr = 10^2$ as compared to $Ri = 100$, $Gr = 10^2$. Moreover, clear results are seen that Nu_{avg} is higher for $Gr = 10^4$ in Figure 4.10(b) compared to $Gr = 10^2$ in Figure 4.10(a) due to high buoyancy forces produced in the cavity. The convection strength seems to be less for decreased Grashof number Gr with all possible cases.

Similar results are also obtained by the influence of Grashof number Gr on the inclined porous cavity. Natural and forced convection regimes are shown in porous medium with $Da = 10^{-4}$ for $Gr = 10^2$ and $Gr = 10^4$. Similar observations are also made in this case. Dominant buoyancy forces are shown by increasing the Grashof number due to which a valuable increment is seen in the form of average Nusselt number Nu_{avg}. So, the effect of Grashof number Gr considered in porous and non- porous medium, observed to be more profound for higher values of Gr in the form of increased heat transfer rate.

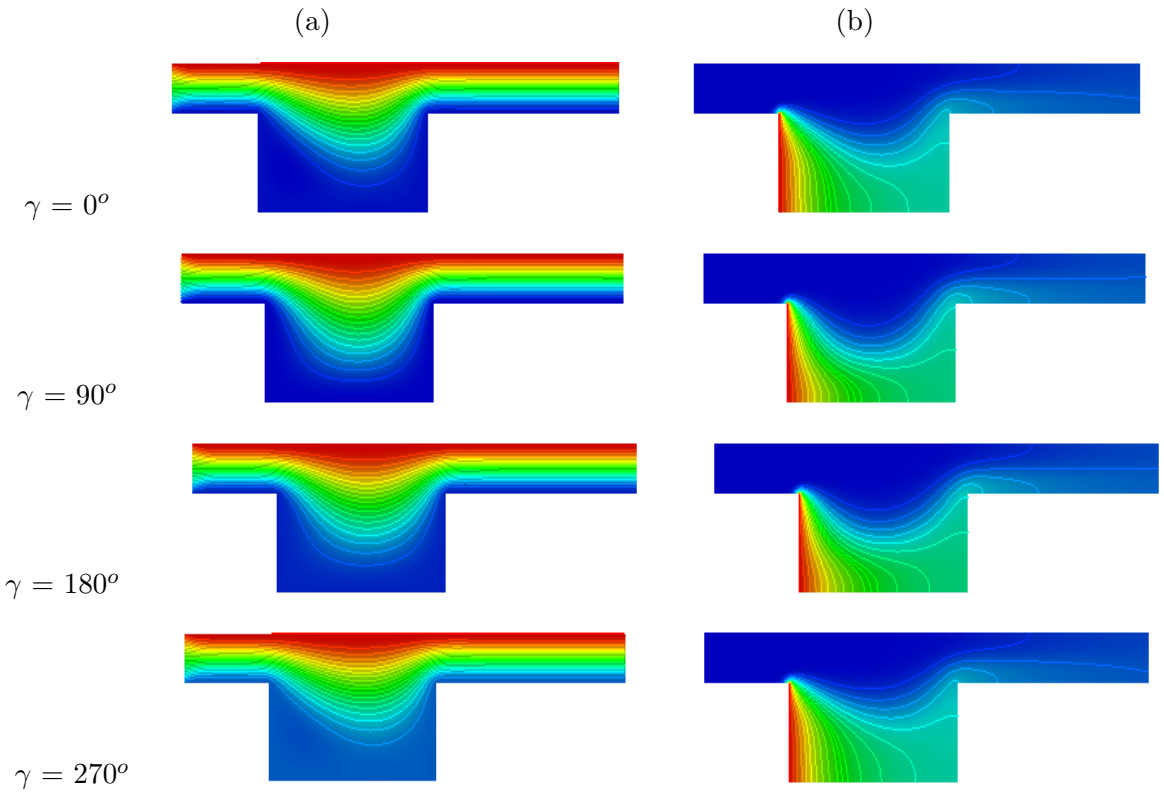

FIGURE 4.2: Influence of different inclination angle γ on (a)streamlines and (b) isotherms with $Ri = 1$, $\phi = 0$, $Re = 10$, $Gr = 10^2$ and $Da = 10^{-4}$.

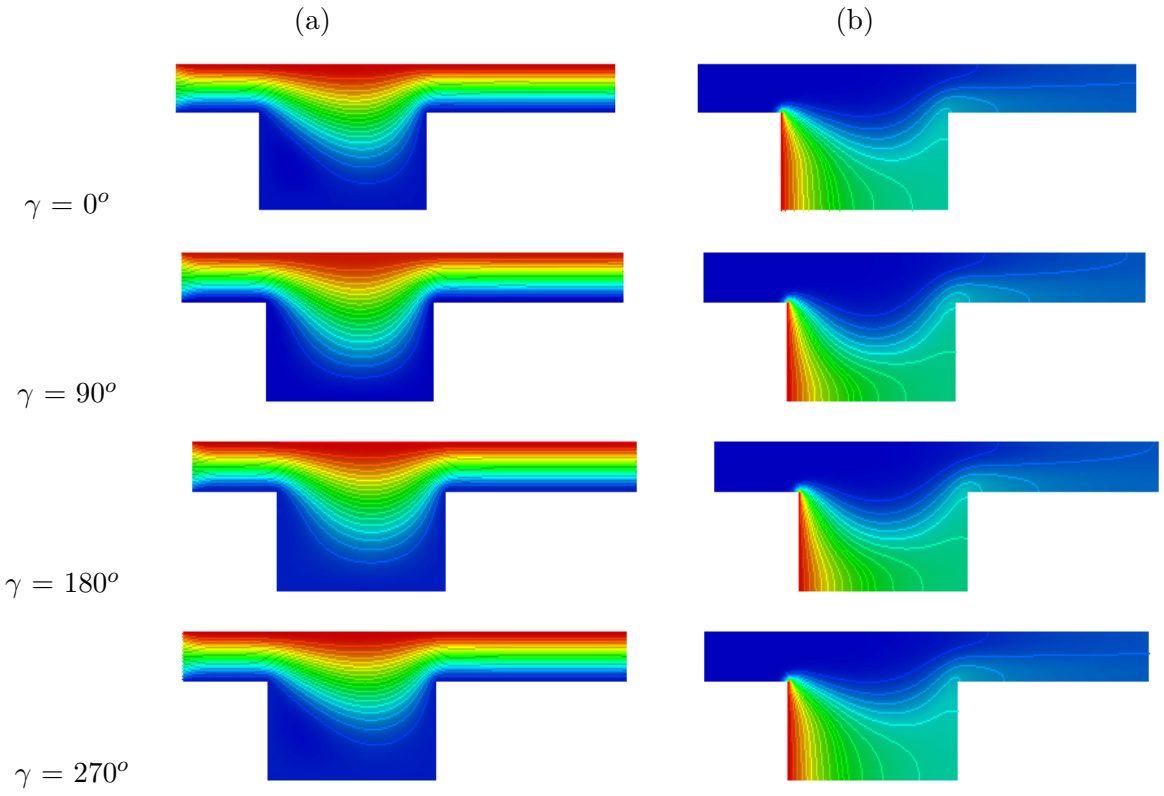

FIGURE 4.3: Influence of different inclination angle γ on (a) streamlines (b) isotherms with $Ri = 1$, $\phi = 0.06$, $Re = 10$, $Gr = 10^2$ and $Da = 10^{-4}$.

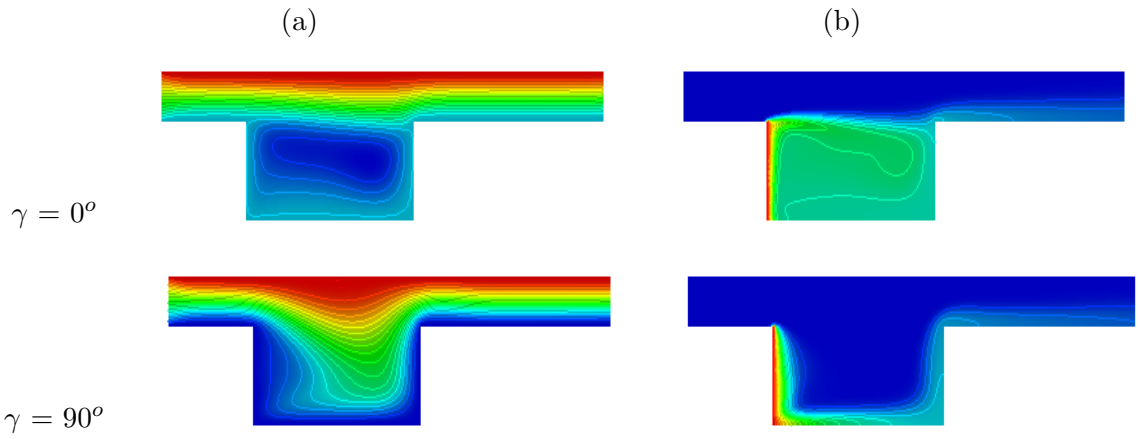

FIGURE 4.4: Influence of different inclination angle γ on (a)streamlines and (b) isotherms with $Ri = 10$, $\phi = 0$,$Re = 50$ and $Da = 10^{-4}$.

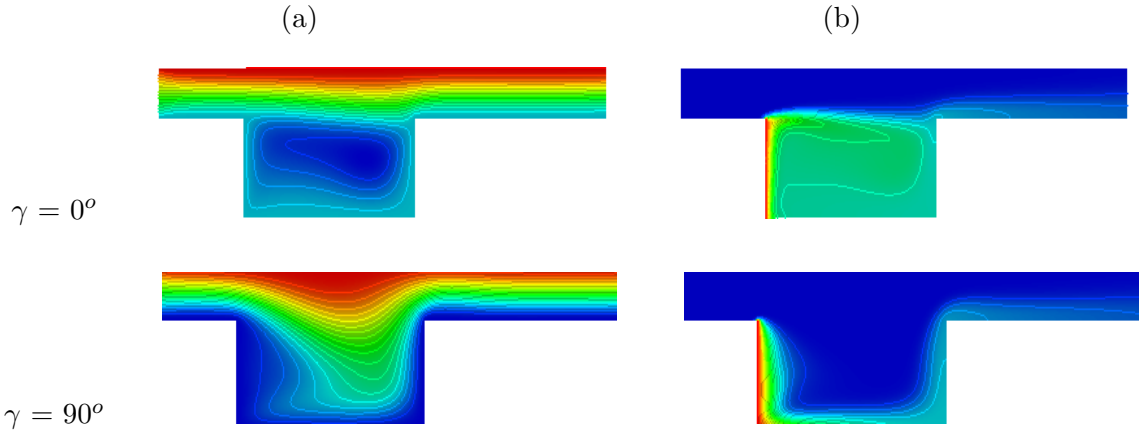

FIGURE 4.5: Influence of different inclination angle γ on (a)streamlines and (b) isotherms with $Ri = 10$, $\phi = 0.06$, $Re = 50$ and $Da = 10^{-4}$.

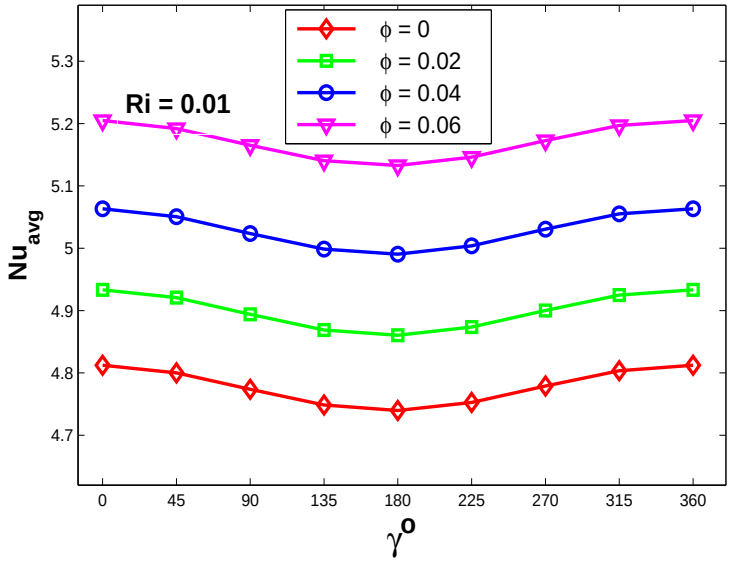

(a)

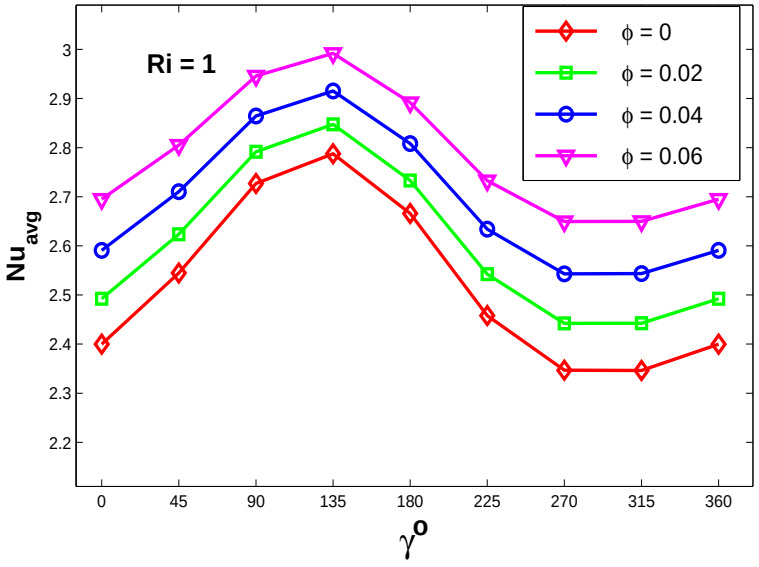

(b)

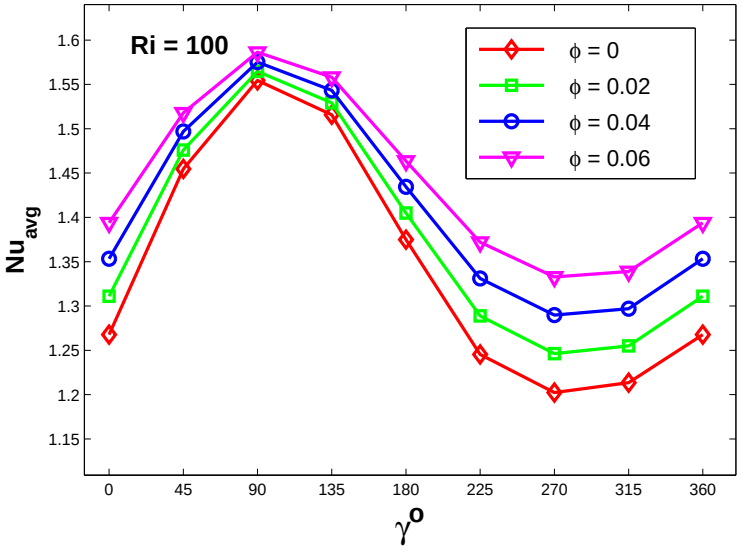

(c)

FIGURE 4.6: Influence of solid volume fraction on the average Nusselt number as a function of inclination angle with Ri at $Da = 10^{-2}$.

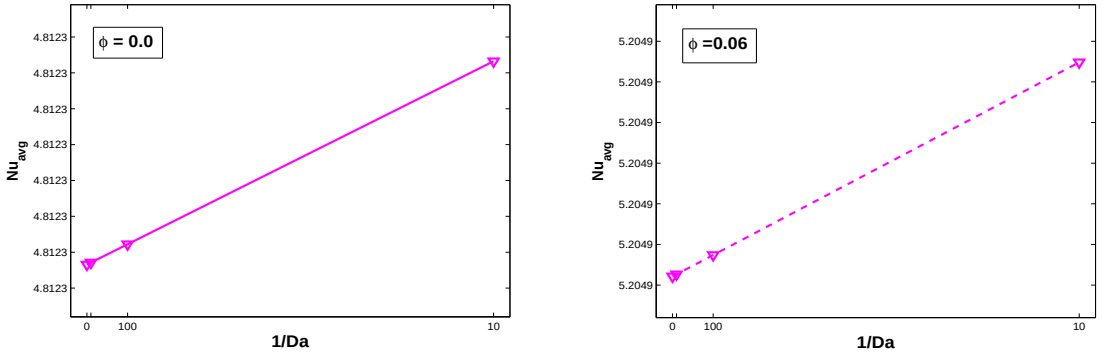

(a) (b)

FIGURE 4.7: Influence of $Da = \infty$, 10^{-3}, 10^{-2}, 10^{-1} of forced convection $Ri = 0.01$ on (a) $\phi = 0$, (b) ϕ=0.06 with $Gr = 10^2$, $\gamma = 0^o$.

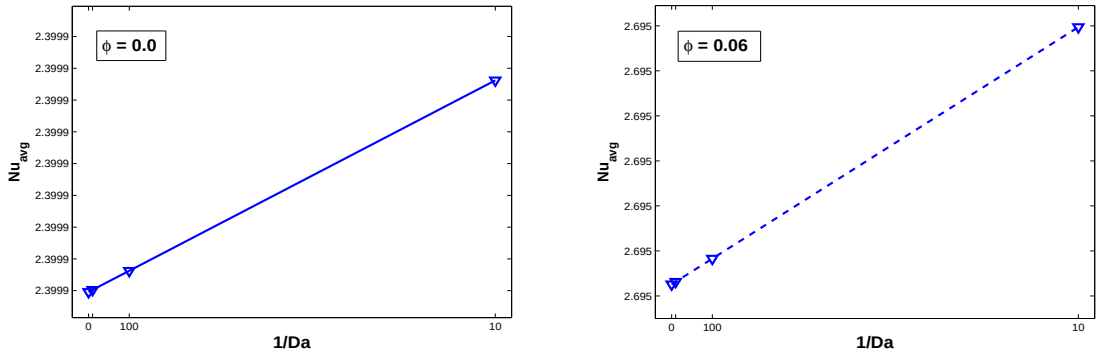

(a) (b)

FIGURE 4.8: Influence of $Da = \infty$, 10^{-3}, 10^{-2}, 10^{-1} of mixed convection $Ri = 1$ on (a) $\phi = 0$, (b) ϕ=0.06 with $Gr = 10^2$, $\gamma = 0^o$.

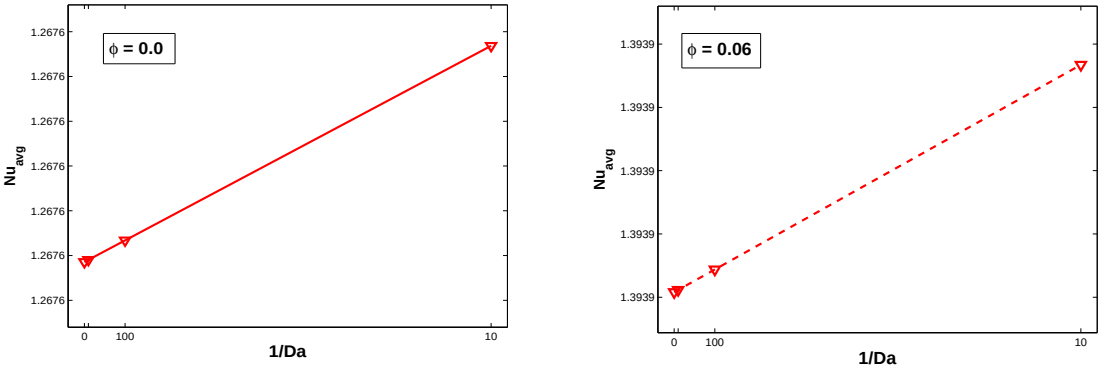

(a) (b)

FIGURE 4.9: Influence of $Da = \infty$, 10^{-3}, 10^{-2}, 10^{-1} of natural convection $Ri = 100$ on (a) $\phi = 0$, (b) ϕ=0.06 with $Gr = 10^2$, $\gamma = 0^o$.

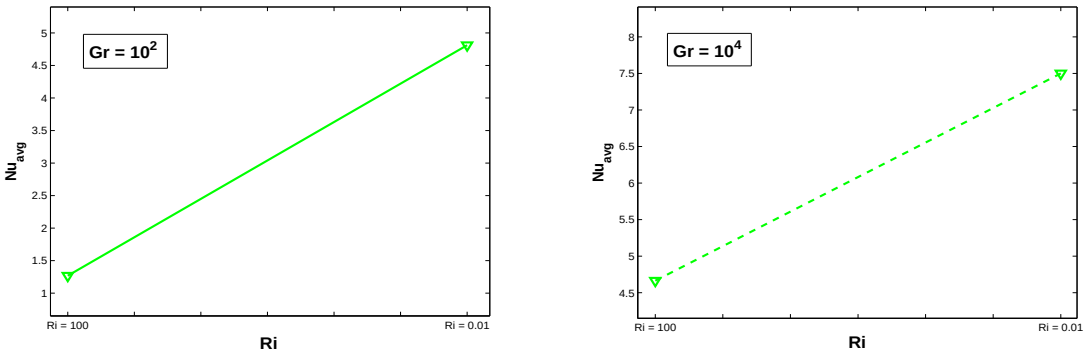

(a) (b)

FIGURE 4.10: Influence of non-porous medium $Da = \infty$ on (a) $Gr = 10^2$, (b) $Gr = 10^4$ with $\gamma = 0^o$ for Ri =100 and 0.01.

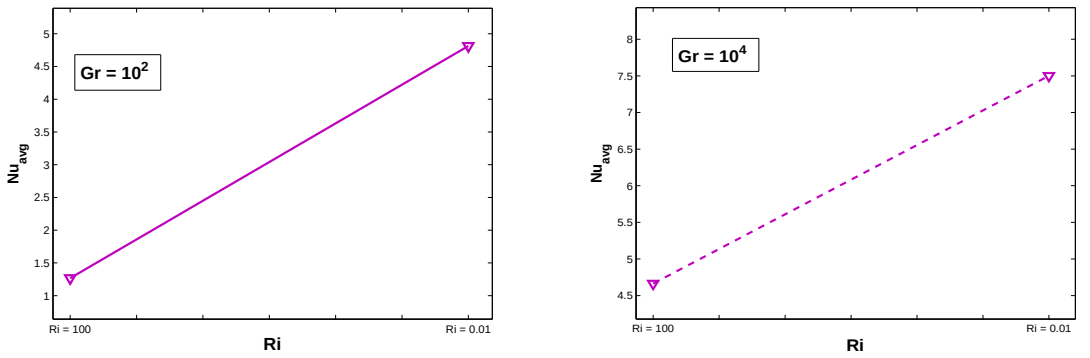

(a) (b)

FIGURE 4.11: Influence of $Da = 10^{-4}$ on (a) $Gr = 10^2$, (b) $Gr = 10^4$ with $\gamma = 0^o$ for Ri =100 and 0.01.

Chapter 5

Conclusion

In this dissertation, the study and analysis of steady and mixed convective flow of the Cu-nanofluid in a inclined channel with open cavity was performed to investigate the effects of Darcy number Da, Grashof number Gr, inclination angle γ and solid volume fraction ϕ on the flow regimes in the form of average Nusselt number Nu_{avg}. The Galerkin finite element approach is implemented for the present problem. Comparisons and results were found to be in good agreement discussed in literature. Graphical illustrations were presented to clarify the conclusions in clear way. Isotherms and streamlines were shown by the variation of inclination angle at 0^o, 90^o, 180^o and 270^o. Researchers used different Darcy models to present their problem for porosity, one of them was analyzed and concluded below.

Problem study is investigated by using Darcy Brinkman model in channel with cavity in inclined plane. Three convection regimes were shown for $Ri = 0.01$, 1 and 100 illustrated graphically by varying inclination angle γ from 0^o to 360^o. It was founded that for $Ri = 0.01$,average Nusselt number is seen to be increased at an angle of 180^o due to dominant shear forces. For $Ri = 1$, greater heat transfer rate is shown at an inclination angle of 135^o. Similarly, for $Ri = 100$, more heat transfer rate is deduced at the angle of 90^o which shows that buoyancy forces strongly effects the fluid flow inside cavity. Furthermore, the average Nusselt number was strongly affected by the increasing values of solid volume fraction ϕ. Increasing the nanofluid particles in the fluid increases the intensity of the fluid which thickens the thermal boundary layer near the heated wall with increasing ratio of solid volume fraction ϕ. Moreover, we obtained various conclusions by varying Darcy number with other parameters. While fixing Grashof number $Gr = 10^2$ and varying the Da in non porous media, heat transfer exchange increases by increasing the porosity for all considered Ri. Concluding all results, following conclusion has been drawn from the study given below.

1. For all considered inclination angles γ, the overall heat transfer rate enhances on increasing the solid volume fraction ϕ in the porous medium.

2. The average Nusselt number Nu_{avg} shows increment with the decrease in Richardson number Ri varies from $(0.01 \leq Ri \leq 100)$.

3. For all considered Ri, heat transfer rate increases with an increase in Darcy number Da with Grashof number $Gr = 10^2$.

4. In non-porous structure for $Da = \infty$, less heat transfer exchange takes place for Grashof number $Gr = 10^2$.

5. Maximum heat transfer exchange is observed for $Gr = 10^4$ as compared to $Gr = 10^2$ while keeping all other parameters constant in porous medium.

Bibliography

[1] O. Manca, S. Nardini, K. Khanafer, and K. Vafai. Effect of heated wall position on mixed convection in a channel with an open cavity. *Numerical Heat Transfer*, 43:259–282, 2003.

[2] O. Manca, S. Nardini, and K. Vafai. Experimental investigation of mixed convection in a channel with an open cavity. *Experimental Heat Transfer*, 19:53–68, 2006.

[3] O. Manca, S. Nardini, and K. Vafai. Experimental investigation of opposing mixed convection in a channel with an open cavity below. *Experimental Heat Transfer*, 21: 99–114, 2008.

[4] M. Rahman, S. Parvin, R. Saidur, and N. Rahim. Magnetohydrodynamic mixed convection in a horizontal channel with an open cavity. *International Communications in Heat and Mass Transfer*, 38:184–193, 2011.

[5] J. Leong, N. Brown, and F. Lai. Mixed convection from an open cavity in a horizontal channel. *International Communications in Heat and Mass Transfer*, 32:583–592, 2005.

[6] Y. Stiriba. Analysis of the flow and heat transfer characteristics for assisting incompressible laminar flow past an open cavity. *International Communications in Heat and Mass Transfer*, 38:901–907, 2011.

[7] Y. Stiriba, J. Ferre, and F. Grau. Heat transfer and fluid flow characteristics of laminar flow past an open cavity with heating from below. *International Communications in Heat and Mass Transfer*, 43:8–15, 2013.

[8] M. Alinia, D. Ganji, and M. Bandpy. Numerical study of mixed convection in an inclined two sided lid driven cavity filled with nanofluid using two-phase mixture model. *International Communications in Heat and Mass Transfer*, 38:1428–1435, 2000.

[9] E. A. Nada and A. Chamkha. Mixed convection flow in a lid-driven inclined square enclosure filled with a nanofluid. *European Journal of Mechanics B/Fluids*, 29:472–482, 2010.

[10] M. A. R. Sharif. Laminar mixed convection in shallow inclined driven cavities with hot moving lid on top and cooled from bottom. *Applied Thermal Engineering*, 27:1036–1042, 2007.

[11] Z. Mehrez, M. Bouterra, A. Cafsi, and A. Belghith. Heat transfer and entropy generation analysis of nanofluids flow in an open cavity. *Computers and Fluids*, 88:363–373, 2013.

[12] Z. Mehrez, M. Bouterra, A. Cafsi, and A. Belghith. Entropy generation and mixed convection in a horizontal channel with an open cavity. *International Journal Energy*, 17:219–239, 2015.

[13] K. M. Khanefar and A. J. Chamkha. Mixed convection flow in a lid driven enclosure filled with a fluid saturated porous medium. *International journal of Heat and Mass Transfer*, 42:2465–2481, 1999.

[14] M. M. Rahman, H. F. Oztop, R. Saidur, S. Mekhilef, and K. A. Salem. Unsteady mixed convection in a porous media filled lid driven cavity heated by a semi circular heaters. *Thermal sciences*, 19:1761–1768, 2015.

[15] E. Vishnuvardhanarao and M. K. Das. Laminar mixed convection in a parallel two sided lid driven differentially heated square cavity filled with a fluid saturated porous medium. *International Journal of Computing and Methodology*, 53:88–110, 2007.

[16] A. A. Hassan and M. A. Ismael. Mixed convection in superposed nanofluid and porous layers inside lid-driven square cavity. *International Journal of Thermal and Environmental Engineering*, 10:93–104, 2015.

[17] A. Hadim and G. Chen. Non-Darcy mixed convection in a vertical porous channel with discrete heat sources at the walls. *International Communication in Heat and Mass Transfer*, 21:377–387, 1994.

[18] S. Sureshkumar and M. Muthtamilselvan. A slanted porous enclosure filled with Cu-water nanofluid. *The European Physical Journal Plus*, 131:95, 2016.

[19] N. Nagarajan and S. Akbar. Heat transfer enhancement of Cu-water nanofluid in a porous square enclosure driven by an incessantly moving flat plate. *Procedia Engineering*, 127:279–286, 2015.

[20] D. S. Kumar, A. K. Dass, and A. Dewan. Analysis of non-Darcy models for mixed convection in a porous cavity using a multigrid approach. *The European Physical Journal Plus*, 56:685–708, 2009.

[21] T. M. Jeng and S. C. Tzeng. Heat transfer in a lid driven enclosure filled with water saturated aluminium foams. *Numerical Heat Transfer*, 54:178–196, 2008.

[22] B. V. R. Kumar and S. Gupta. Free convection in a non-Darcian wavy porous enclosure. *International Journal Engineering Sciences*, 41:1827–1848, 2003.

[23] B. V. R. Kumar and S. Gupta. Free convection in a thermally stratified non-Darcian wavy enclosure. *Journal porous media*, 07:261–277, 2004.

[24] X. Chen, J. M. Li, W. T. Dai, and B. X. Wang. Exchanging convection heat transfer in mini tubes with nanoparticles suspensions. *Journal Engineering Thermophysics*, 25: 643–645, 2004.

[25] R. Nasrin and M. A. Alim. A slanted porous enclosure filled with Cu-water nanofluid. *Heat Transfer - Asian Research*, 04:42, 2013.

[26] N. Atalla and F. Sgard. Finite element and boundary methods in structural acoustics and vibration. *Taylor and Francis group*, 2015.

[27] J. N. Reddy. An introduction to the finite element method (Third Ed.) Mcgraw-Hill. 03, 2006.

[28] Z. Mehrez, A. Cafsi, A. Belghith, and P. Quere. The entropy generation analysis in the mixed convective assisting flow of Cu-water nanofluid in an inclined open cavity. *Advanced Powder Technology*, 1:10, 2015.

[29] M. Aminossadati and B. Ghasemi. A numerical study of mixed convection in a horizontal channel with a discrete source in an open cavity. *Euorepean Journal of mechanics B/Fluids*, 28:590–598, 2009.

[30] S. Hussain, F. Schieweck, and S. Turek. Efficient Newton multigrid solutiontechniques for higher order space time Galerkin discretizations of incompressible flow. *Applied Numerical Mathematics*, 83:51–71, 2014.